nature immunology

C13orf31 (FAMIN) is a central regulator of immunometabolic function

M Zaeem Cader[1], Katharina Boroviak[2], Qifeng Zhang[3], Ghazaleh Assadi[4], Sarah L Kempster[1], Gavin W Sewell[1], Svetlana Saveljeva[1], Jonathan W Ashcroft[1], Simon Clare[2], Subhankar Mukhopadhyay[2], Karen P Brown[5], Markus Tschurtschenthaler[1], Tim Raine[1], Brendan Doe[2], Edwin R Chilvers[6], Jules L Griffin[7], Nicole C Kaneider[1], R Andres Floto[5,6], Mauro D'Amato[4,8], Allan Bradley[2], Michael J O Wakelam[3], Gordon Dougan[2] & Arthur Kaser[1]

Single-nucleotide variations in *C13orf31* (*LACC1*) that encode p.C284R and p.I254V in a protein of unknown function (called 'FAMIN' here) are associated with increased risk for systemic juvenile idiopathic arthritis, leprosy and Crohn's disease. Here we set out to identify the biological mechanism affected by these coding variations. FAMIN formed a complex with fatty acid synthase (FASN) on peroxisomes and promoted flux through *de novo* lipogenesis to concomitantly drive high levels of fatty-acid oxidation (FAO) and glycolysis and, consequently, ATP regeneration. FAMIN-dependent FAO controlled inflammasome activation, mitochondrial and NADPH-oxidase-dependent production of reactive oxygen species (ROS), and the bactericidal activity of macrophages. As p.I254V and p.C284R resulted in diminished function and loss of function, respectively, FAMIN determined resilience to endotoxin shock. Thus, we have identified a central regulator of the metabolic function and bioenergetic state of macrophages that is under evolutionary selection and determines the risk of inflammatory and infectious disease.

Immunological and inflammatory diseases arise from complex environment–gene interactions. While the external triggers remain unknown, human genetic studies have revealed the genomic-risk 'landscapes' of these conditions. Genes encoding proteins with established immunological function have been predictably identified as plausible candidates at various risk loci. The mechanistic contribution of their polymorphic variants to disease pathophysiology has been addressed experimentally for a few of these genes, although this is currently based largely on conjecture for most. Furthermore, for a large number of risk loci and genes, it remains entirely unclear how their products are mechanistically involved in disease, including some for which no biological function is known yet at all. We hypothesized that studying uncharacterized gene products singled out by genetic disease association might reveal novel biological mechanisms that are important not only for human health but also for mammalian biology in general.

Two coding polymorphisms in *C13orf31* (*LACC1*), an open reading frame that encodes a protein of unknown function, render this gene and its product particularly notable. First, homoallelic carriage of a rare missense mutation at g.43,883,879T>C, which leads to substitution of arginine for cysteine at position 284 (p.C284R), has been linked in consanguineous families to systemic juvenile idiopathic arthritis (sJIA) (a periodic fever syndrome) and to early-onset Crohn's disease (CD) (an inflammatory bowel disease)[1,2]. Second, the haplotype identified by the common single-nucleotide polymorphism (SNP) rs3764147 (g.43,883,789A>G), which leads to substitution of valine for isoleucine at position 254 (p.I254V), has been associated with increased risk for leprosy (an infection caused by *Mycobacterium leprae*) and CD[3,4].

Here we found that the protein encoded by that open reading frame served as 'rheostat' for the synthesis of endogenous fatty acids and their mitochondrial oxidation and thereby controlled glycolytic activity and overall ATP regeneration. As a consequence, the product of this polymorphic gene determined the mitochondrial and nicotinamide adenine dinucleotide phosphate (NADPH)-oxidase-dependent production of reactive oxygen species (ROS), bactericidal activity and inflammasome activation in macrophages. These findings prompted us to call this protein 'FAMIN' ('fatty acid metabolism–immunity nexus').

RESULTS

Interaction of FAMIN with fatty acid synthase

C13orf31 mRNA has its highest expression in macrophages and is predicted to encode a cytoplasmic protein of 430 amino acids that lacks similarity to other mammalian protein families[5,6]. We performed

[1]Division of Gastroenterology and Hepatology, Department of Medicine, Addenbrooke's Hospital, University of Cambridge, Cambridge, UK. [2]Wellcome Trust Sanger Institute, Wellcome Trust Genome Campus, Hinxton, UK. [3]Signalling Programme, Babraham Institute, Babraham Research Campus, Cambridge, UK. [4]Department of Biosciences and Nutrition, Karolinska Institutet, Stockholm, Sweden. [5]Cambridge Institute for Medical Research, University of Cambridge, Cambridge Centre for Lung Infection, Cambridge, UK. [6]Division of Respiratory Medicine, Department of Medicine, Addenbrooke's and Papworth Hospitals, University of Cambridge, Cambridge, UK. [7]Department of Biochemistry, University of Cambridge, Cambridge, UK. [8]BioDonostia Health Research Institute San Sebastian and Ikerbasque, Basque Foundation for Science, Bilbao, Spain. Correspondence should be addressed to A.K. (ak729@cam.ac.uk).

Received 9 May; accepted 1 July; published online 1 August 2016; doi:10.1038/ni.3532

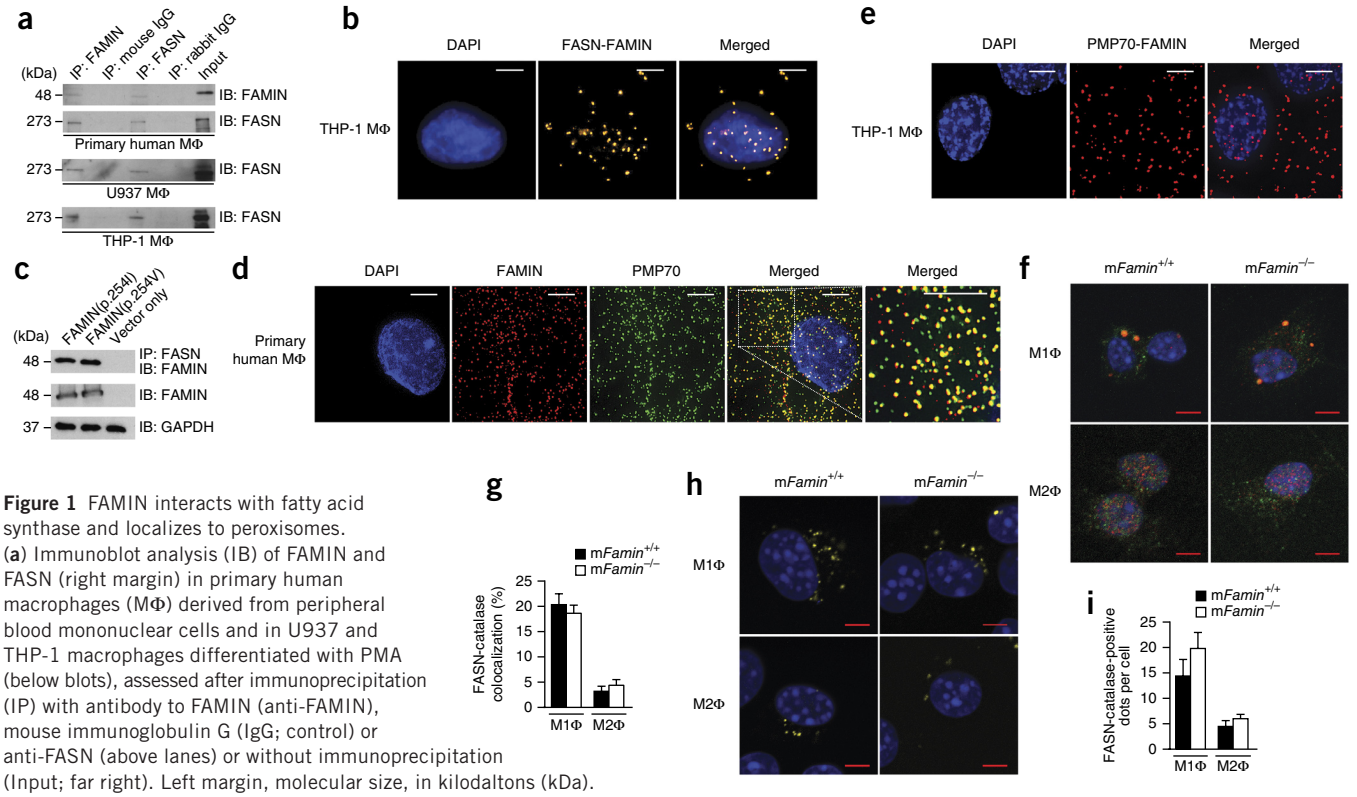

Figure 1 FAMIN interacts with fatty acid synthase and localizes to peroxisomes. (**a**) Immunoblot analysis (IB) of FAMIN and FASN (right margin) in primary human macrophages (MΦ) derived from peripheral blood mononuclear cells and in U937 and THP-1 macrophages differentiated with PMA (below blots), assessed after immunoprecipitation (IP) with antibody to FAMIN (anti-FAMIN), mouse immunoglobulin G (IgG; control) or anti-FASN (above lanes) or without immunoprecipitation (Input; far right). Left margin, molecular size, in kilodaltons (kDa). (**b**) PLA of FAMIN and FASN (yellow) in THP-1 macrophages also stained with the DNA-binding dye DAPI (blue throughout). (**c**) Immunoblot analysis of FAMIN or GAPDH (loading control) in lysates of HEK293 cells transfected to express human FAMIN(p.254I) or FAMIN(p.254V) or with vector alone (above lanes), assessed with (top blot) or without (bottom two blots) immunoprecipitation with anti-FASN. (**d**) Immunofluorescence analysis of the co-localization of FAMIN (red) with PMP70 (green) in primary human macrophages (enlarged from areas outlined in **Supplementary Fig. 2a**); far right, enlargement of the area outlined at left. (**e**) PLA of FAMIN and PMP70 (red) in THP-1 macrophages. (**f**) Immunofluorescence analysis of the co-localization of FASN (red) with catalase (green) in m*Famin*$^{+/+}$ and m*Famin*$^{-/-}$ M1 macrophages (M1Φ) and M2 macrophages (M2Φ). (**g**) Quantification of the results in **f**. (**h**) PLA of FASN and catalase (yellow) in m*Famin*$^{+/+}$ and m*Famin*$^{-/-}$ M1 and M2 macrophages. (**i**) Quantification of the results in **h**. Scale bars (**b**,**d**–**f**,**h**), 5 μm. Data are representative of three independent experiments (**a**–**e**) or one experiment with three mice and six cells (**f**,**g**) or ten cells (**h**,**i**) imaged per sample (**f**–**i**; mean + s.e.m.).

an unbiased proteomics search for interaction partners to begin to elucidate FAMIN's function. After discounting proteins involved in the synthesis, folding and degradation of proteins or cytoskeletal organization, we found that fatty acid synthase (FASN; EC 2.3.1.85) was the most abundant peptide detected with FAMIN tagged with Strep-tag at the amino or carboxyl terminus, expressed as 'bait' in HEK293T human embryonic kidney cells (**Supplementary Fig. 1** and **Supplementary Table 1**). Endogenous FAMIN reciprocally immunoprecipitated together with FASN in lysates of primary human monocytes differentiated into macrophages, as well as in lysates of THP-1 and U937 human monocytic cell lines differentiated into macrophages (**Fig. 1a**). A proximity-ligation assay (PLA) further confirmed the co-localization of FAMIN and FASN *in situ* (**Fig. 1b**). The two common polymorphic FAMIN variants with either isoleucine (p.254I) or valine (p.254V) at amino acid position 254 exhibited equivalent interaction with FASN in co-immunoprecipitation experiments with lysates of HEK293T cells transfected with vector expressing FAMIN (**Fig. 1c**), which further confirmed that FAMIN was in a complex with FASN.

Mammalian FASN is a large cytoplasmic polypeptide multienzyme central to *de novo* lipogenesis (DNL)[7]. FASN associates with membranes in various subcellular compartments[8]. We therefore performed confocal microscopy to determine the intracellular localization of FAMIN in macrophages differentiated from primary human monocytes and THP-1 cells. Immunofluorescence analysis revealed nearly perfect co-localization of FAMIN with the peroxisome markers PMP70 and catalase (**Fig. 1d** and **Supplementary Fig. 2a–c**), while it had little co-localization with other organelle markers (**Supplementary Fig. 2d**,**e**). Co-localization between FAMIN and PMP70 was confirmed by PLA (**Fig. 1e** and **Supplementary Fig. 2f**); this confirmed the peroxisomal localization of FAMIN.

Peroxisomes are organelles involved in lipid metabolism that are closely associated with lipid droplets and mitochondria[9]. Macrophages exhibit metabolic and functional plasticity, epitomized by *in vitro* culture under non-polarizing (M0), classical (M1) or alternative (M2) activation conditions[10]. While aerobic glycolysis is a defining characteristic of 'inflammatory' M1 macrophages and is their chief mechanism for the generation of ATP[11], 'regenerative' M2 macrophages rely on mitochondrial fatty-acid oxidation (FAO; also called 'β-oxidation') to fuel oxidative phosphorylation[12]. To study FAMIN's function, we generated mice in which we knocked out alleles of *Lacc1* (*9030625A04Rik*, the mouse homolog of the human gene *C13orf31*; called 'm*Famin*' here)[13] (**Supplementary Fig. 3**). Similar to FAMIN, FASN does not have a peroxisomal localization motif and has been shown to form a complex with PMP70 on the cytoplasmic side of peroxisomes[9,14]. Consistent with that, we found that a portion of cellular FASN immunoreactivity localized together with catalase-positive peroxisomes in m*Famin*$^{+/+}$ M1 macrophages (20% ± 3% (mean ± s.e.m.)) and M2 macrophages (4% ± 2%), and this was not

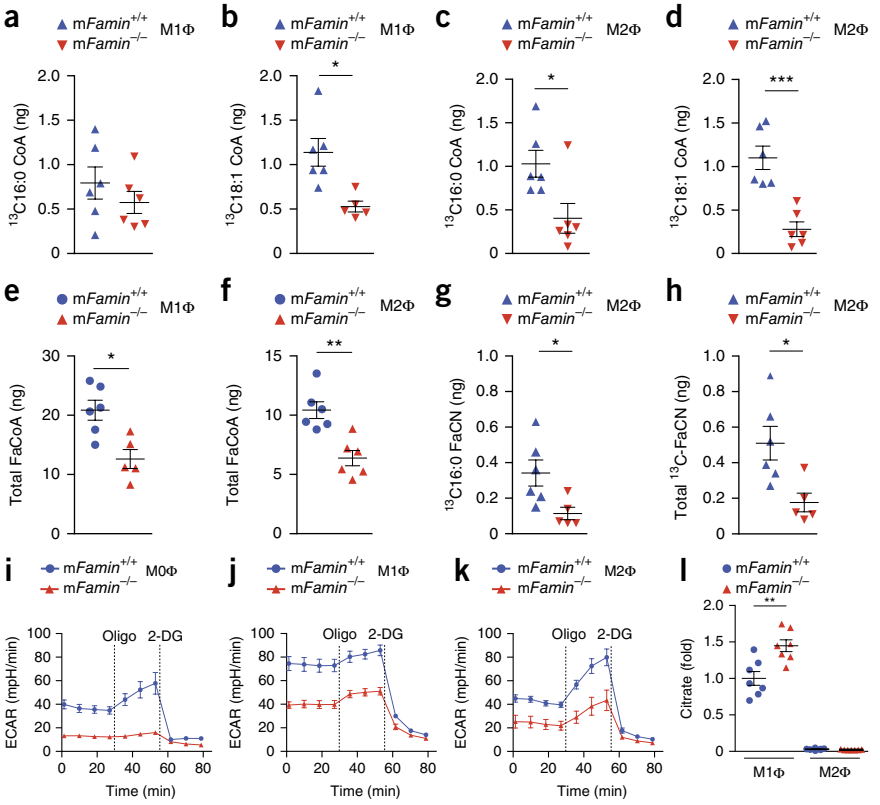

Figure 2 FAMIN promotes glycolysis and flux of glucose into *de novo* lipogenesis. (**a**–**d**) Quantification of ^{13}C-labeled C16:0 fatty acyl-CoA (**a**,**c**) and C18:1 fatty acyl-CoA (**b**,**d**) in m*Famin*$^{+/+}$ and m*Famin*$^{-/-}$ M1 macrophages (**a**,**b**) and M2 macrophages (**c**,**d**) after a 24-hour pulse with 1,2-^{13}C-glucose. (**e**,**f**) Quantification of total fatty acyl CoA in m*Famin*$^{+/+}$ and m*Famin*$^{-/-}$ M1 macrophages (**e**) and M2 macrophages (**f**). (**g**,**h**) Quantification of ^{13}C-labeled C16:0 fatty-acyl carnitine (FaCN) (**g**) and total fatty-acyl carnitine (**h**) in m*Famin*$^{+/+}$ and m*Famin*$^{-/-}$ M2 macrophages pulsed as in **a**–**d**. (**i**–**k**) ECAR of m*Famin*$^{+/+}$ and m*Famin*$^{-/-}$ M0 macrophages (**i**), M1 macrophages (**j**) and M2 macrophages (**k**) given sequential treatment (dotted vertical lines) with oligomycin (Oligo) and 2-deoxyglucose (2-DG). (**l**) Quantification of citrate in m*Famin*$^{+/+}$ and m*Famin*$^{-/-}$ M1 and M2 macrophages; results are presented relative to those of m*Famin*$^{+/+}$ M1 macrophages, set as 1. Each symbol (**a**–**h**,**l**) represents an individual mouse; small horizontal lines indicate the mean (± s.e.m.). $^{*}P < 0.05$, $^{**}P < 0.01$ and $^{***}P < 0.001$ (unpaired, two-tailed Student's *t*-test; Grubb's test outlier exclusion). Data are from one experiment with six mice (**a**–**h**) or seven mice (**l**) or one experiment with three mice representative of three independent experiments (**i**–**k**; mean ± s.e.m.).

affected by the absence of FAMIN (**Fig. 1f**,**g**). PLA confirmed those spatial relationships (**Fig. 1h**,**i**). Bone-marrow-derived macrophages cultured under M0, M1 or M2 conditions all expressed m*Famin* mRNA, with the highest expression in cells differentiated under M1 conditions (**Supplementary Fig. 4a**). Expression of *Fasn* mRNA was similar in m*Famin*$^{+/+}$ macrophages and m*Famin*$^{-/-}$ macrophages, with the highest expression in cells cultured under M2 conditions (**Supplementary Fig. 4b**). In addition, expression of FASN protein was also equivalent in m*Famin*$^{+/+}$ M1 and M2 macrophages and their m*Famin*$^{-/-}$ counterparts (**Supplementary Fig. 4c**). Together our data indicated that FAMIN and FASN formed a complex on peroxisomes and that the peroxisomal localization of FASN, particularly prominent in M1 macrophages, was not impaired in m*Famin*$^{-/-}$ cells.

Control of carbon flux via DNL by FAMIN

FASN catalyzes all steps in the synthesis of long-chain saturated fatty acids (LCFAs) (predominantly C16:0 palmitic acid)[15]. This enzymatic reaction utilizes cytoplasmic acetyl–coenzyme A (acetyl-CoA), malonyl-CoA (generated from acetyl-CoA by carboxylation) and NADPH[15]. Cytoplasmic acetyl-CoA is itself generated by ATP citrate lyase after the export of mitochondrial citrate formed during glucose- or amino-acid-fueled Krebs-cycle activity[16]. In consequence, FASN function allows the storage of excess energy, derived from glucose and amino-acid oxidation, in lipid droplets after the activation of LCFA and its esterification to LCFA-CoA and thence to triacylglycerol[17]. FASN also synthesizes fatty-acyl moieties of membrane lipids and provides the precursors of many other cellular and signaling lipids. Given the diverse functions of lipid moieties that are dependent on FASN function, precise channeling of its products into distinct metabolic pathways is essential[15,17].

To assess FASN activity *in situ*, we pulse labeled mouse bone-marrow-derived macrophages with [$^{13}C_{1,2}$]-glucose (**Supplementary Fig. 5a**). Uptake of ^{13}C into total LCFAs and palmitic acid was below the limit of detection in m*Famin*$^{+/+}$ and m*Famin*$^{-/-}$ M1 and M2 macrophages (data not shown), consistent with limited turnover and exogenous uptake of the large pools of free fatty acids. However, we did observe incorporation of ^{13}C into C16:0 and C18:1 fatty-acyl-CoA esters (the activated forms of LCFAs used for lipid synthesis and mitochondrial oxidation) in m*Famin*$^{+/+}$ M1 and M2 macrophages (**Fig. 2a**–**d**). Together these data indicated that newly synthesized fatty acids were immediately esterified to CoA for subsequent use and thus did not determine the abundance of the free-fatty-acid pool. Furthermore, we discovered that the incorporation of ^{13}C into C18:1-CoA in M1 macrophages and into C16:0-CoA and C18:1-CoA in M2 macrophages was much lower in m*Famin*$^{-/-}$ cells than in m*Famin*$^{+/+}$ cells (**Fig. 2a**–**d**). The abundance of total LCFA-CoA was also significantly lower in m*Famin*$^{-/-}$ M1 and M2 macrophages than in their m*Famin*$^{+/+}$ counterparts (**Fig. 2e**,**f**), while total fatty-acid content, including palmitic acid, was predictably indistinguishable in cells of these genotypes (**Supplementary Table 2**). Together these data indicated that FAMIN determined, via DNL, the availability of fatty-acyl-CoA for processes such as FAO.

FAO requires the transport of CoA-activated LCFAs across mitochondrial membranes as acyl-carnitine esters[18]. The exchange of CoA for carnitine by the cytoplasmic carnitine palmitoyltransferase CPT1a is the rate-limiting step of FAO[18]. Consistent with the diminished specific availability of fatty-acyl-CoA, the incorporation of [$^{13}C_{1,2}$]glucose-derived ^{13}C into fatty-acyl carnitine species (total and C16:0) was much lower in m*Famin*$^{-/-}$ M2 macrophages than in m*Famin*$^{+/+}$ M2 macrophages (**Fig. 2g**,**h**), while its incorporation was below the limit of detection in M1 macrophages (data not shown). Notably, while the incorporation of glucose-derived ^{13}C into acyl-CoA was substantial after a 24-hour pulse (~20–30% of C16:0-CoA and C18:1-CoA in m*Famin*$^{+/+}$ M2 macrophages), it was low

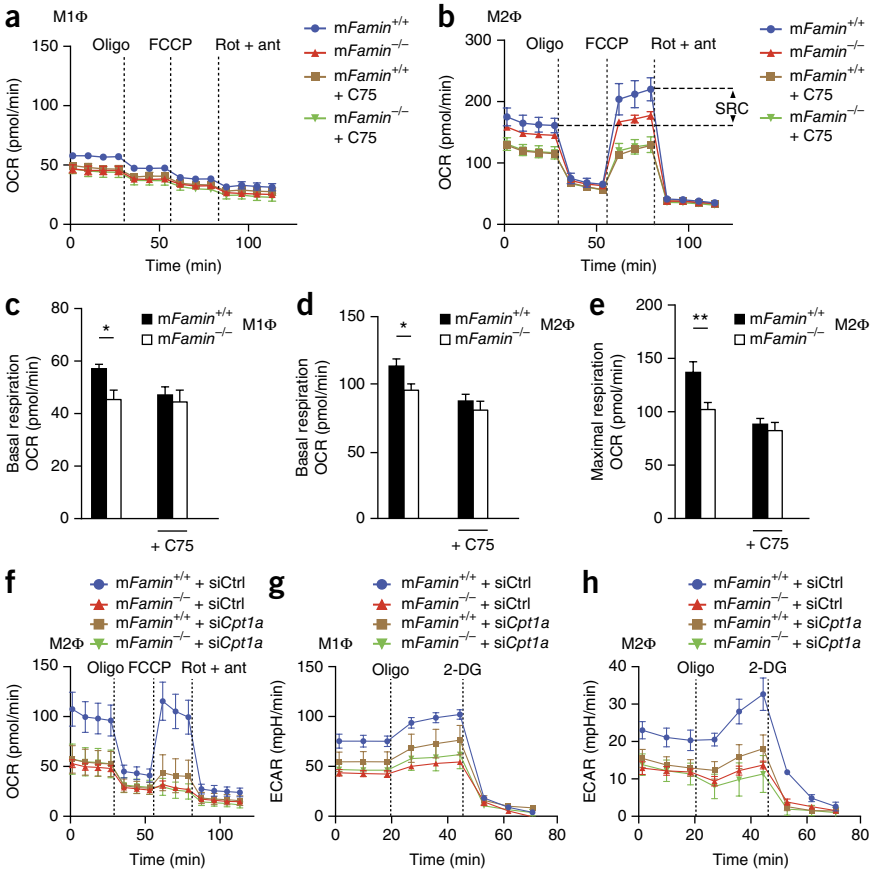

Figure 3 FAMIN augments FAO. (**a**,**b**) OCR of m*Famin*$^{+/+}$ and m*Famin*$^{-/-}$ M1 macrophages (**a**) and M2 macrophages (**b**) in the presence (+ C75) or absence of 20 μM C75 (key), during sequential treatment (dotted vertical lines) with oligomycin, FCCP and rotenone plus antimycin (Rot + ant). Dashed horizontal lines (**b**) indicate SRC. (**c**–**e**) Basal respiratory capacity (as OCR) (**c**,**d**) and maximal respiratory capacity (**e**) in m*Famin*$^{+/+}$ and m*Famin*$^{-/-}$ M1 macrophages (**c**; $n = 6$ mice) and M2 macrophages (**d**,**e**; $n = 14$ mice (m*Famin*$^{+/+}$; no C75), 13 mice (m*Famin*$^{-/-}$; no C75), 9 mice (m*Famin*$^{+/+}$; C75 present) or 7 mice (m*Famin*$^{-/-}$; C75 present)) in the presence or absence of C75 (horizontal axes). (**f**–**h**) OCR (**f**) and ECAR (**g**,**h**) of m*Famin*$^{+/+}$ and m*Famin*$^{-/-}$ M1 macrophages (**g**) and M2 macrophages (**f**,**h**) treated with *Cpt1a*-specific small interfering RNA (siRNA) (si*Cpt1a*) or control siRNA with a scrambled sequence (siCtrl) and given sequential treatment as in **a** (**f**) or with oligomycin and 2-deoxyglucose (**g**,**h**). $^{*}P < 0.05$ and $^{**}P < 0.01$ (unpaired, two-tailed Student's *t*-test). Data are from one experiment with three mice representative of three independent experiments (**a**,**b**,**f**–**h**; mean ± s.e.m.) or are pooled from two or more independent experiments (**c**–**e**; mean + s.e.m.).

for acyl carnitine species (~4% of total acyl carnitine in m*Famin*$^{+/+}$ M2 macrophages) at the same time point (**Fig. 2g**,**h**). Collectively, these results indicated FAMIN directly controlled the flux of glucose-derived carbon into DNL and onward into acyl carnitine, with the latter possibly involving an intermediary step via triacylglycerols[12].

Control of glycolysis by FAMIN via DNL

To determine whether loss of FAMIN consequently influenced glycolytic metabolism in macrophages, we measured the extracellular acidification rate (ECAR), an indicator of glycolysis[19], in wild-type and mutant macrophages. We found that the ECAR was much lower in m*Famin*$^{-/-}$ M1 macrophages than in m*Famin*$^{+/+}$ M1 macrophages, with a similar proportional decrease from the expected lower baseline in M0 and M2 macrophages (**Fig. 2i**–**k**). The difference in the ECAR was further enhanced after blockade of the F_0 subunit of mitochondrial ATP synthase with oligomycin A (**Fig. 2i**–**k**), which stimulates the alternative generation of ATP via glycolysis[20]. This observation indicated that FAMIN-dependent glycolysis was maximized under conditions in which mitochondrial respiration was uncoupled from ATP synthesis. Differences between m*Famin*$^{+/+}$ macrophages and m*Famin*$^{-/-}$ macrophages in their ECAR were abolished after inhibition of glycolysis with 2-deoxy-D-glucose (**Fig. 2i**–**k**). Similarly, measurement of ECAR in the presence of exogenous pyruvate, which bypasses glycolysis, showed that the ECAR of m*Famin*$^{-/-}$ macrophages was indistinguishable from that of m*Famin*$^{+/+}$ macrophages (**Supplementary Fig. 5b**). Together these data demonstrated that FAMIN determined the baseline and maximal glycolytic capacity of macrophages. Notably, the intracellular concentration of citrate, which itself inhibits glycolysis at the level of phosphofructokinase[21], was substantially higher in m*Famin*$^{-/-}$ macrophages differentiated under M1 conditions than in their m*Famin*$^{+/+}$ counterparts (**Fig. 2l**). The abundance of Krebs-cycle intermediates other than citrate in m*Famin*$^{-/-}$ M1 and M2 macrophages remained indistinguishable from that in their m*Famin*$^{+/+}$ counterparts (**Supplementary Fig. 5c**), which indicated an absence of direct effects of FAMIN on Krebs-cycle activity. Collectively, these results indicated that the impairment in glycolysis might have been a consequence of defective DNL.

Promotion of mitochondrial FAO by FAMIN

Since we had observed that the extent of carbon flux through DNL into acyl carnitine was determined by FAMIN, we hypothesized that FAMIN might control mitochondrial FAO. As expected, m*Famin*$^{+/+}$ M2 macrophages had high basal oxidative phosphorylation, as reflected by their high oxygen-consumption rate (OCR), whereas M1 macrophages had a low OCR that was refractory to treatment with oligomycin, an inhibitor of ATP synthase (**Fig. 3a**–**d**). Impaired glycolysis usually leads to a compensatory increase in oxidative phosphorylation for the maintenance of ATP intracellular concentrations[22]. However, in addition to their defective glycolysis, m*Famin*$^{-/-}$ M1 and M2 macrophages also concomitantly exhibited significantly lower basal OCR than that of their m*Famin*$^{+/+}$ counterparts (**Fig. 3a**–**d**). Maximal uncontrolled OCR (MU-OCR) is elicited by dissipation of the mitochondrial electrochemical proton gradient with the mitochondrial uncoupler FCCP (carbonyl-cyanide *p*-tri-fluoro-methoxy-phenylhydrazone), which also 'unmasks' the spare respiratory capacity (SRC) (the difference between maximal capacity and basal respiratory capacity)[12]. The MU-OCR was diminished and SRC could not be elicited in m*Famin*$^{-/-}$ M2 macrophages following uncoupling via FCCP (**Fig. 3b**,**e**). Complete inhibition of mitochondrial respiration via rotenone and antimycin A (inhibitors of electron-transport chain complexes I and III, respectively) abolished the differences between m*Famin*$^{-/-}$macrophages and m*Famin*$^{+/+}$ macrophages in their OCR

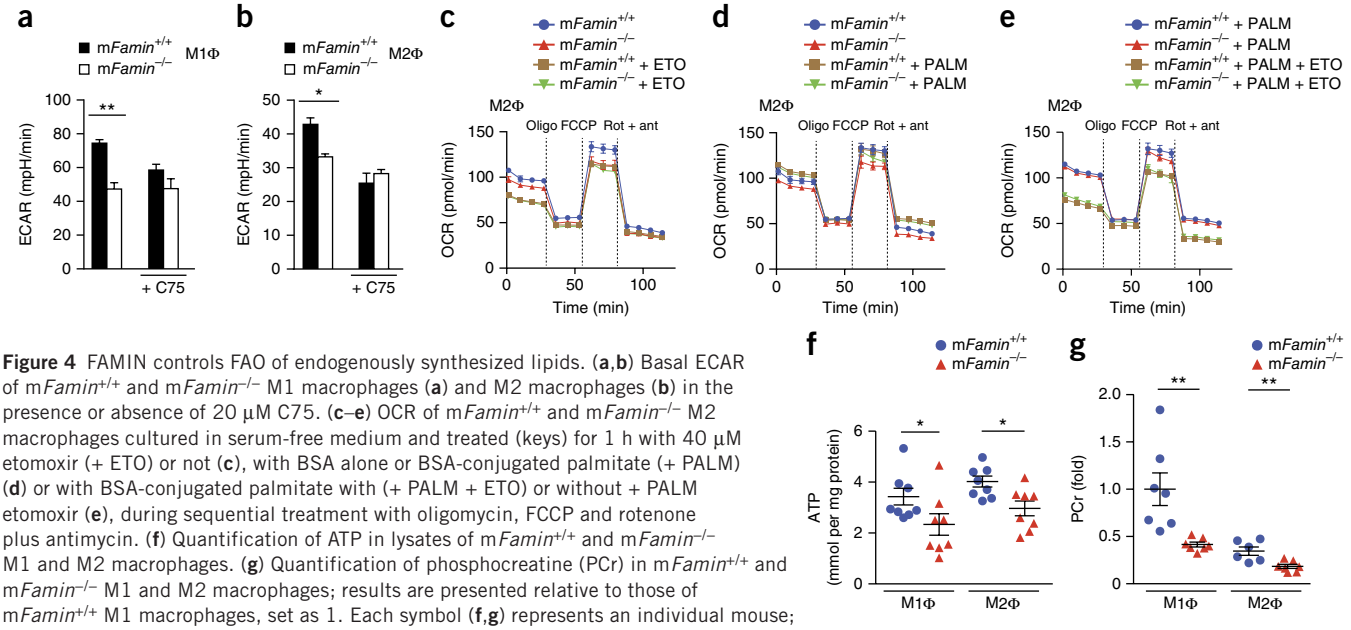

Figure 4 FAMIN controls FAO of endogenously synthesized lipids. (**a**,**b**) Basal ECAR of m*Famin*$^{+/+}$ and m*Famin*$^{-/-}$ M1 macrophages (**a**) and M2 macrophages (**b**) in the presence or absence of 20 μM C75. (**c**–**e**) OCR of m*Famin*$^{+/+}$ and m*Famin*$^{-/-}$ M2 macrophages cultured in serum-free medium and treated (keys) for 1 h with 40 μM etomoxir (+ ETO) or not (**c**), with BSA alone or BSA-conjugated palmitate (+ PALM) (**d**) or with BSA-conjugated palmitate with (+ PALM + ETO) or without + PALM etomoxir (**e**), during sequential treatment with oligomycin, FCCP and rotenone plus antimycin. (**f**) Quantification of ATP in lysates of m*Famin*$^{+/+}$ and m*Famin*$^{-/-}$ M1 and M2 macrophages. (**g**) Quantification of phosphocreatine (PCr) in m*Famin*$^{+/+}$ and m*Famin*$^{-/-}$ M1 and M2 macrophages; results are presented relative to those of m*Famin*$^{+/+}$ M1 macrophages, set as 1. Each symbol (**f**,**g**) represents an individual mouse; small horizontal lines indicate the mean (± s.e.m.). $*P < 0.05$ and $**P < 0.01$ (unpaired, two-tailed Student's *t*-test). Data are from one experiment with three mice representative of three independent experiments (**a**–**e**; mean ± s.e.m.) or are from one experiment with eight mice (**f**) or seven mice (**g**).

(**Fig. 3a**,**b**). Together these data demonstrated that m*Famin*$^{-/-}$ M1 and M2 macrophages exhibited diminished oxidative capacity in not only basal respiratory states but also uncoupled respiratory states.

A high basal OCR and SRC in M2 macrophages has been reported to be secondary to FAO[12]. We therefore considered defective FAO as the cause for the impaired OCR that was particularly apparent in m*Famin*$^{-/-}$ M2 macrophages. To test the hypothesis that FAMIN specifically affects mitochondrial FAO and not oxidative phosphorylation fueled by other substrates, we inhibited the activity of CPT1a. Genetic silencing of *Cpt1a* or blocking CPT1a with the irreversible inhibitor etomoxir[23] decreased the OCR in m*Famin*$^{+/+}$ M2 macrophages to that in m*Famin*$^{-/-}$ M2 macrophages (**Fig. 3f** and **Supplementary Fig. 5d**). Notably, silencing *Cpt1a* in m*Famin*$^{+/+}$ M1 and M2 macrophages reduced their basal ECAR to the low ECAR in m*Famin*$^{-/-}$ macrophages, while silencing *Cpt1a* in m*Famin*$^{-/-}$ cells did not diminish the ECAR any further (**Fig. 3g**,**h**). In summary, our findings demonstrated that loss of FAMIN led to decreased FAO that was needed to sustain high rates of glycolysis.

FAMIN controls FAO of endogenously synthesized lipids

Given our finding that FAMIN controlled the flux of carbon from glucose into acyl-CoA, we hypothesized that FAMIN might facilitate FAO of *de-novo*-synthesized fatty acids. Blockade of FASN's function with the small-molecule synthetic inhibitor C75 (ref. 24) decreased the basal OCR and SRC in m*Famin*$^{+/+}$ M2 macrophages and abolished the differences between m*Famin*$^{+/+}$ cells and m*Famin*$^{-/-}$ cells in OCR and SRC (**Fig. 3a**–**e**). Notably, blockade of FASN with C75 decreased ECAR in both m*Famin*$^{+/+}$ M1 macrophages and m*Famin*$^{+/+}$ M2 macrophages and abolished the m*Famin*-genotype-related differences in ECAR (**Fig. 4a**,**b**). To provide further support for those findings, we measured OCR under conditions devoid of exogenous lipids, in which FAO is thus entirely dependent upon lipids synthesized *de novo* by FASN. As observed under lipid-replete conditions above, baseline OCR and MU-OCR were lower in m*Famin*$^{-/-}$ M2 macrophages than in m*Famin*$^{+/+}$ M2 macrophages during culture in the absence of exogenous lipids, and these differences were abolished by inhibition of CPT1a with etomoxir (**Fig. 4c**). Supplementation with exogenous palmitic acid increased the basal OCR and MU-OCR in m*Famin*$^{-/-}$ M2 macrophages to levels equivalent to those in m*Famin*$^{+/+}$ M2 macrophages (**Fig. 4d**), which demonstrated that exogenous palmitic acid was able to 'rescue' the lower basal and maximum OCR in 'starved' m*Famin*$^{-/-}$ M2 macrophages. Finally, blockade of CPT1a in M2 macrophages supplemented with exogenous palmitic acid decreased the basal OCR and MU-OCR in m*Famin*$^{+/+}$ cells to rates identical to those in m*Famin*$^{-/-}$ cells (**Fig. 4e**). These data demonstrated that FAMIN supported FAO and glycolysis via a mechanism that involved DNL.

Control of macrophage energy stores by FAMIN

Given that FAMIN controlled the extent of FAO and glycolysis in parallel and, notably, that these processes did not 'cross-compensate' for each other's diminished function, we hypothesized that FAMIN's function would affect macrophage energy stores. The total cellular ATP was much lower in bone-marrow-derived m*Famin*$^{-/-}$ M1 and M2 macrophages than in their m*Famin*$^{+/+}$ counterparts (a decrease of 30% ± 12% and 26% ± 6% (mean ± s.e.m.), respectively; **Fig. 4f**). The concentration of cellular phosphocreatine, a rapidly mobilizable energy store, was similarly lower in m*Famin*$^{-/-}$ M1 and M2 macrophages than in their m*Famin*$^{+/+}$ counterparts (**Fig. 4g**). Transmission electron microscopy demonstrated morphological changes in the mitochondria of m*Famin*$^{-/-}$ macrophages, characterized by elongation and narrowing (consistent with adaptation in response to ATP depletion), relative to the morphology of mitochondria in m*Famin*$^{+/+}$ macrophages[25] (**Fig. 5a**,**b**). Hence, FAMIN promoted glycolysis, FAO and, consequently, cellular energy stores in macrophages.

FAMIN and macrophage ROS production

Mitochondrial respiration generates ROS when electrons prematurely escape electron-transport-chain complexes I and III and react with molecular oxygen to generate superoxide anions[26]. Consistent with diminished mitochondrial oxidation in the absence of FAMIN, the abundance of mitochondrial ROS (mROS) was much lower in m*Famin*$^{-/-}$ M1 and M2 macrophages than in their m*Famin*$^{+/+}$

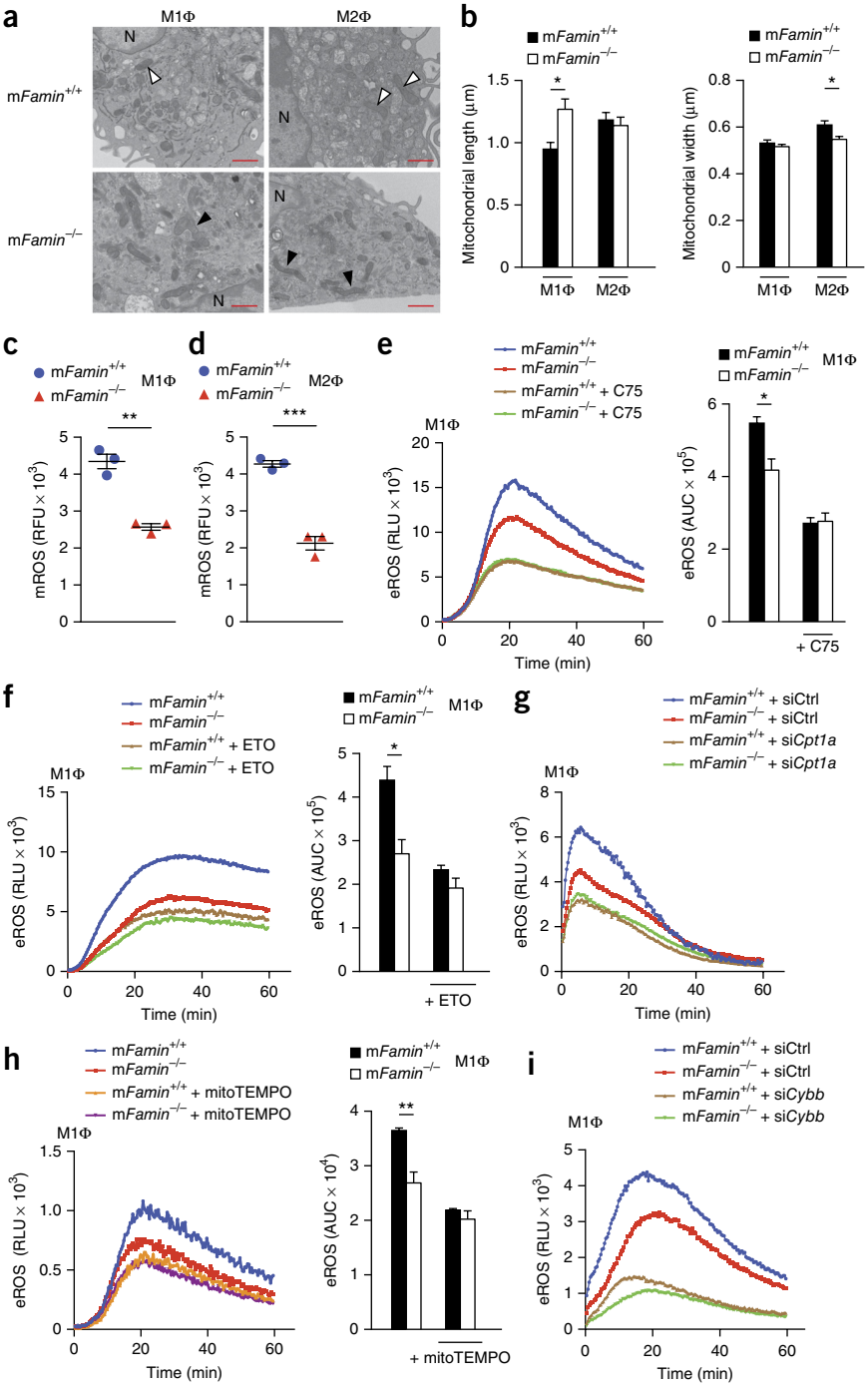

Figure 5 FAMIN-deficient macrophages have impaired mROS production and exhibit features of mitochondrial injury and remodeling. (**a**) Transmission electron microscopy of m*Famin*$^{+/+}$ and m*Famin*$^{-/-}$ M1 and M2 macrophages; arrowheads indicate mitochondria. N, nucleus. Scale bars, 1 μm. (**b**) Mitochondrial length and width in cells as in **a**. (**c**,**d**) mROS in unstimulated m*Famin*$^{+/+}$ and m*Famin*$^{-/-}$ M1 macrophages (**c**) and M2 macrophages (**d**) stained with a red fluorescent mitochondrial superoxide indicator; results are presented in relative fluorescence units (RFU). (**e**–**i**) eROS production in m*Famin*$^{+/+}$ and m*Famin*$^{-/-}$ M1 macrophages left untreated or treated for 16 h with 20 μM C75 (**e**), for 1 h with 40 μM etomoxir (**f**) or for 1 h with a scavenger of mitochondrial superoxide (500 μM mitoTEMPO) (**h**), or treated with control siRNA (**g**,**i**) or *Cpt1a*-specific siRNA (**g**) or *Cybb*-specific siRNA (si*Cybb*) (**i**), all followed by stimulation with zymosan; results are presented as relative light units (RLU) (left) or as the area under the curve (AUC) (right, **e**,**f**,**h**). Each symbol (**c**,**d**) represents an individual mouse; small horizontal lines indicate the mean (± s.e.m.). $^{*}P < 0.05$ and $^{**}P < 0.01$ (Mann–Whitney *U*-test (**b**) or unpaired, two-tailed Student's *t*-test (**c**–**f**,**h**)). Data are representative of one experiment with three mice and six cells per sample (**a**,**b**; mean + s.e.m.) or are from one experiment with three mice representative of at least two independent experiments (**c**–**i**; mean + s.e.m.).

counterparts, as assessed by a red-fluorescent indicator of mitochondrial superoxide (**Fig. 5c**,**d**). The abundance of cytoplasmic ROS was also lower in m*Famin*$^{-/-}$ M1 macrophages than in m*Famin*$^{+/+}$ M1 macrophages, as measured with the cytosolic ROS indicator CM-H_2DCFDA, although this parameter did not differ between these genotypes in M2 macrophages (**Supplementary Fig. 6a**,**b**). Stimulation with the Toll-like receptor 2 agonist zymosan resulted in significantly less production of extracellular ROS (eROS) in m*Famin*$^{-/-}$ M1 and M2 macrophages than in their m*Famin*$^{+/+}$ counterparts (**Fig. 5e** and **Supplementary Fig. 6c**). Inhibition of FASN with C75 or silencing of *Fasn* through the use of small interfering RNA approximately halved the production of eROS in m*Famin*$^{+/+}$ macrophages polarized under M1 or M2 conditions and abrogated the m*Famin*-associated differences (**Fig. 5e** and **Supplementary Fig. 6c**–**e**). Inhibition of CPT1a with etomoxir diminished the zymosan-elicited generation of eROS in m*Famin*$^{+/+}$ macrophages to levels observed in m*Famin*$^{-/-}$ cells, regardless of whether the latter were treated with etomoxir or not (**Fig. 5f** and **Supplementary Fig. 6f**). A similar pattern of eROS production was observed after silencing of *Cpt1a* (**Fig. 5g** and **Supplementary Fig. 6g**) and, notably, after scavenging of mROS (**Fig. 5h** and **Supplementary Fig. 6h**). As expected, the production of eROS was dependent on the gp91^{phox} NADPH oxidase[27], since silencing the gene encoding gp91^{phox} (*Cybb*) largely abolished the m*Famin*-genotype-related differences (**Fig. 5i** and **Supplementary Fig. 6i**). Notably, m*Famin*$^{-/-}$ macrophages exhibited diminished generation of eROS relative to that of m*Famin*$^{+/+}$ macrophages despite greater availability of NADPH in m*Famin*$^{-/-}$ macrophages than in m*Famin*$^{+/+}$ macrophages (**Supplementary Fig. 6j**). In contrast to results obtained for macrophages, the production of eROS elicited by the phorbol ester PMA in mouse neutrophils was independent of FAMIN (**Supplementary Fig. 6k**), consistent with absence of m*Famin* expression in mouse neutrophils[6] (data not shown). In summary, FAMIN controlled mROS production via a DNL- and FAO-dependent mechanism and mROS, in turn, determined the capacity of the NADPH oxidase system to elicit eROS in macrophages.

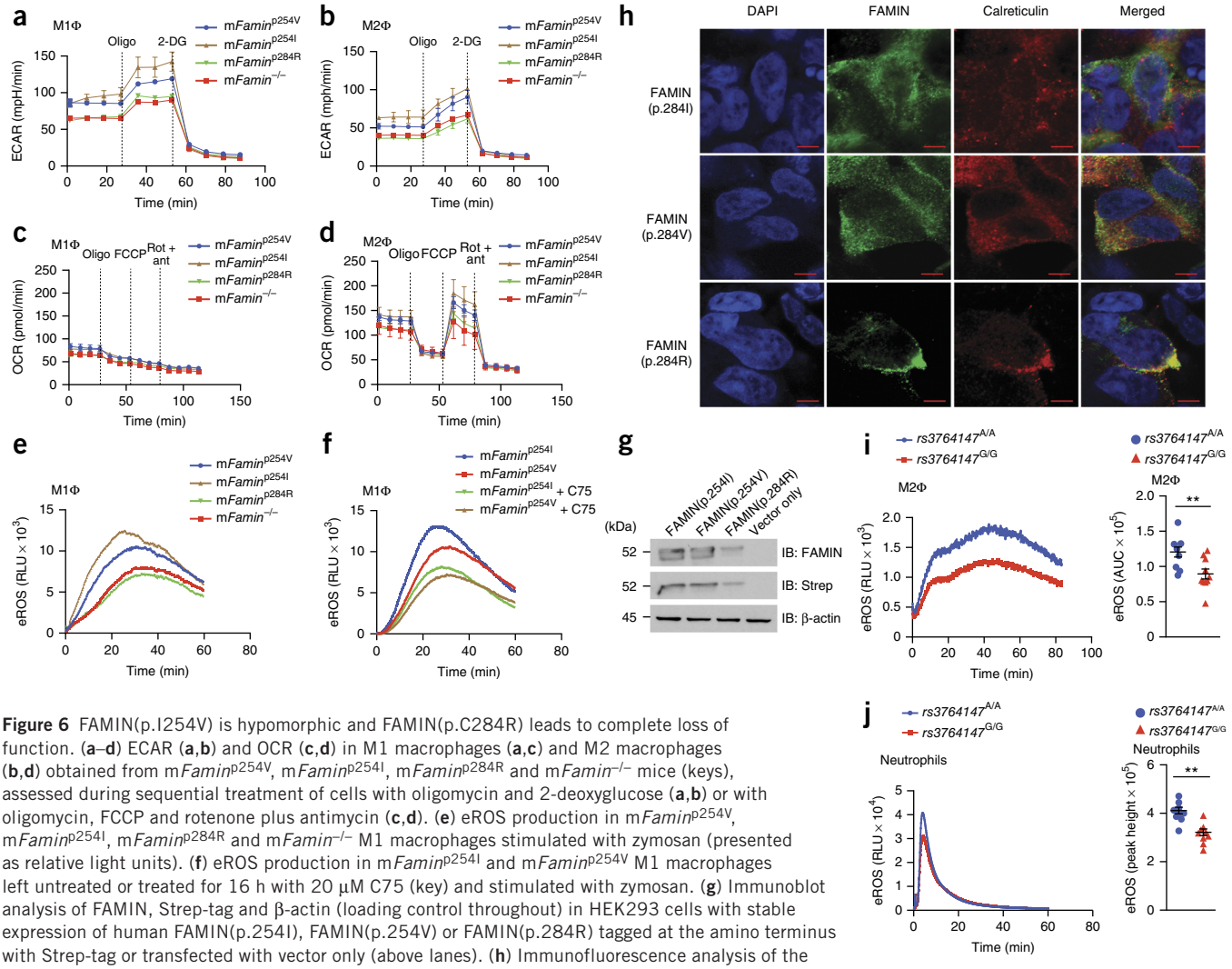

Figure 6 FAMIN(p.I254V) is hypomorphic and FAMIN(p.C284R) leads to complete loss of function. (**a**–**d**) ECAR (**a**,**b**) and OCR (**c**,**d**) in M1 macrophages (**a**,**c**) and M2 macrophages (**b**,**d**) obtained from m*Famin*^{p254V}, m*Famin*^{p254I}, m*Famin*^{p284R} and m*Famin*$^{-/-}$ mice (keys), assessed during sequential treatment of cells with oligomycin and 2-deoxyglucose (**a**,**b**) or with oligomycin, FCCP and rotenone plus antimycin (**c**,**d**). (**e**) eROS production in m*Famin*^{p254V}, m*Famin*^{p254I}, m*Famin*^{p284R} and m*Famin*$^{-/-}$ M1 macrophages stimulated with zymosan (presented as relative light units). (**f**) eROS production in m*Famin*^{p254I} and m*Famin*^{p254V} M1 macrophages left untreated or treated for 16 h with 20 μM C75 (key) and stimulated with zymosan. (**g**) Immunoblot analysis of FAMIN, Strep-tag and β-actin (loading control throughout) in HEK293 cells with stable expression of human FAMIN(p.254I), FAMIN(p.254V) or FAMIN(p.284R) tagged at the amino terminus with Strep-tag or transfected with vector only (above lanes). (**h**) Immunofluorescence analysis of the co-localization of FAMIN (green) and calreticulin (red) in HEK293 cells as in **g** (left margin). Scale bars, 5 μm. (**i**) eROS production in M2 macrophages derived from peripheral blood mononuclear cells of healthy donors ($n = 10$) homozygous for the 'risk haplotype' (*rs3764147*$^{G/G}$) or 'protective haplotype' (*rs3764147*$^{A/A}$) for CD and leprosy, stimulated *in vitro* with zymosan. (**j**) eROS production in PMA-stimulated neutrophils (genotypes as in **i**), presented as relative light units (left) or peak height (right). Each symbol (**i**,**j**) represents an individual donor; small horizontal lines indicate the mean (± s.e.m.). $^*P < 0.05$ and $^{**}P < 0.01$ (unpaired, two-tailed Student's *t*-test). Data are from one experiment with three mice representative of two independent experiments (**a**–**f**; mean ± s.e.m. in **a**–**d**), are representative of three independent experiments (**g**,**h**) or are pooled from ten independent experiments (**i**,**j**).

Impaired function of FAMIN p.I254V and p.C284R

We next investigated whether the metabolic mechanisms elucidated above were affected by genetic variation in m*Famin*. Wild-type C57BL/6N mice have the human 'risk' nucleotide guanine that encodes valine at the corresponding amino acid position 254 (called 'm*Famin*^{p254V}' here). Using the CRISPR-Cas9 gene-editing system, we introduced single-nucleotide exchanges and generated mice homozygous for the nucleotide (adenosine) that is protective against leprosy and CD and that encodes isoleucine at amino acid position 254 (m*Famin*^{p254I})[28] (**Supplementary Fig. 3**). We also generated mice homozygous for the nucleotide (cytosine) at position g.43,883,879 that encodes arginine at amino acid position 284 (the rare m*Famin*^{p284R} variant linked to monogenic sJIA and early-onset CD in consanguineous families) instead of the highly conserved cytosine at that position (m*Famin*^{p284C}) (**Supplementary Fig. 3**). Metabolic flux was equivalent in m*Famin*^{p284R} macrophages and m*Famin*$^{-/-}$ macrophages, while m*Famin*^{p254I} macrophages exhibited the highest ECAR, basal OCR and MU-OCR, and m*Famin*^{p254V} macrophages had intermediate levels of these (**Fig. 6a**–**d**). Consistent with such diminished function and loss of function for FAMIN(p.I254V) and FAMIN(p.C284R), respectively, zymosan elicited greater production of eROS from m*Famin*^{p254I} macrophages than from m*Famin*^{p254V} cells, while eROS production in m*Famin*^{p284R} was diminished similar to its decrease in m*Famin*$^{-/-}$ macrophages (**Fig. 6e** and **Supplementary Fig. 7a**). The genotype-related differences between m*Famin*^{p254I} macrophages and m*Famin*^{p254V} macrophages in zymosan-elicited production of eROS were abolished by the inhibition of FASN with C75 (**Fig. 6f** and **Supplementary Fig. 7b**). Overexpression of human FAMIN(p.254I) under control of a cytomegalovirus promoter in HEK293T cells yielded FAMIN expression indistinguishable from that of cells transfected with a construct encoding FAMIN(p.254V) (**Fig. 6g**), while expression of FAMIN(p.284R) was low and FAMIN(p.284R) localized together with calreticulin (**Fig. 6g**,**h**), indicative of retention in the endoplasmic reticulum. Together our results demonstrated that the substitution p.C284R

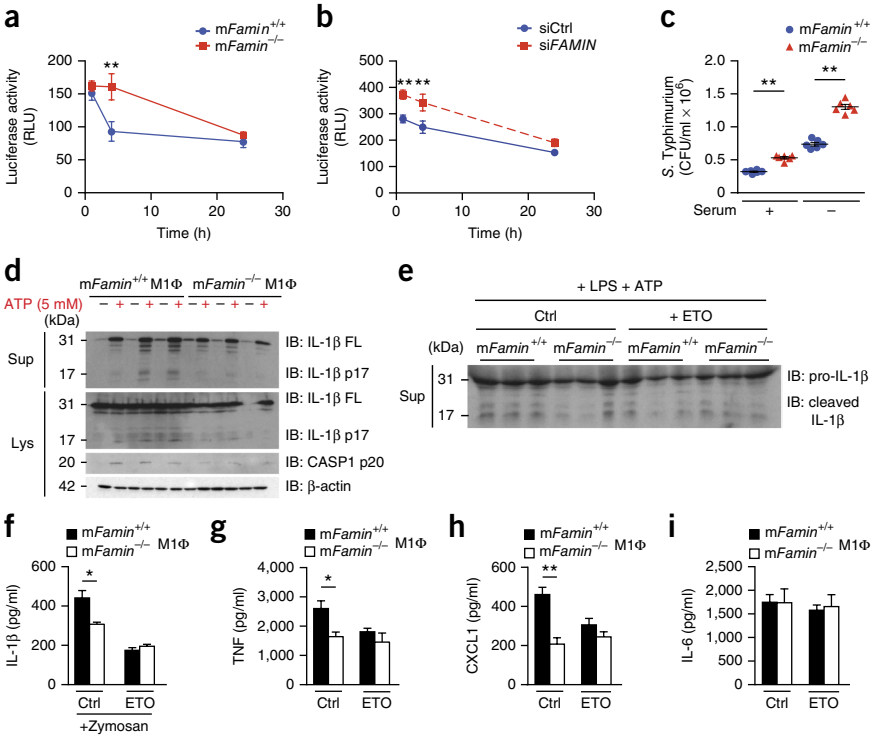

Figure 7 FAMIN deficiency causes defective bacterial clearance and inflammasome activation *in vitro*. (**a**) Luciferase activity of m*Famin*$^{+/+}$ and m*Famin*$^{-/-}$ M0 macrophages at 0, 4, or 24 h after infection with BCG expressing a luciferase-reporter-encoding gene; results are presented as relative light units. (**b**) Luciferase activity of M0 macrophages derived from human peripheral blood mononuclear cells and treated with *FAMIN*-specific siRNA (si*FAMIN*) or control siRNA with a scrambled sequence (siCtrl), after infection as in **a**. (**c**) Bacterial load in m*Famin*$^{+/+}$ and m*Famin*$^{-/-}$ M0 macrophages infected with *Salmonella enterica* serovar Typhimurium SL1344 (*S.* Typhimurium) in serum-containing (+) or serum-free (–) medium; results are presented as colony-forming units (CFU). Each symbol represents an individual mouse; small horizontal lines indicate the mean (± s.e.m.). (**d**) Immunoblot analysis of full-length (FL) or cleaved (p17) IL-1β and cleaved active caspase-1 (CASP1 p20) in supernatants (Sup) and lysates (Lys) of m*Famin*$^{+/+}$ and m*Famin*$^{-/-}$ M1 macrophages pretreated for 2 h with LPS (500 ng/ml) in serum-free medium and left unstimulated (–) or stimulated (+) for 15 min with ATP (above lanes). (**e**) Immunoblot analysis of pro-IL-1β and cleaved IL-1β in supernatants of M1 macrophages pretreated and stimulated as in **d** in the presence (+ ETO) or absence (Ctrl) of 100 μM etomoxir. (**f**) Concentration of IL-1β in supernatants of M1 macrophages given no pretreatment or pre-treated for 2 h with 100 μM etomoxir (horizontal axis) and stimulated with zymosan (200 μg/ml). (**g**–**i**) Concentration of TNF (**g**), CXCL1 (**h**) and IL-6 (**i**) in supernatants of M1 macrophages pre-treated with etomoxir or not as in **f** (horizontal axes) and stimulated with LPS (1 μg/ml). $^{*}P < 0.05$ and $^{**}P < 0.01$ (one-way analysis of variance with *post-hoc* Bonferroni's test (**a**,**b**) or unpaired, two-tailed Student's *t*-test (**c**,**f**–**i**)). Data are from one experiment with three mice representative of three independent experiments (**a**,**d**–**i**; mean ± s.e.m. in **a** and mean + s.e.m. in **f**–**i**) or are from one experiment with six independent samples per group (**b**,**c**; mean ± s.e.m.).

caused complete loss of FAMIN function, while the single methyl-group change in p.I254V resulted in diminished FAMIN function.

We next obtained peripheral blood from healthy humans homozygous for the haplotype linked to greater risk of CD and leprosy (rs3764147$^{G/G}$) and the haplotype that is protective against leprosy and CD (rs3764147$^{A/A}$). We isolated primary neutrophils and monocytes from the donors and differentiated the latter *in vitro* into macrophages under M2 conditions. The expression of *FAMIN* mRNA in rs3764147$^{G/G}$ M2 macrophages was indistinguishable from that in rs3764147$^{A/A}$ M2 macrophages (**Supplementary Fig. 7c**). Human rs3764147$^{G/G}$ M2 macrophages exhibited less zymosan-elicited production of eROS than that of rs3764147$^{A/A}$ M2 macrophages (**Fig. 6i**). In contrast to mouse neutrophils, human neutrophils expressed FAMIN[5] (data not shown). Treatment with PMA triggered lower ROS production in rs3764147$^{G/G}$ neutrophils than in rs3764147$^{A/A}$ neutrophils (**Fig. 6j**); this extended the diminished function that resulted from the rs3764147$^{G/G}$ beyond macrophages. These data demonstrated that the 'risk haplotype' for CD and leprosy (rs3764147$^{G/G}$) was associated with decreased production of eROS. This was a phenocopy of our results obtained with macrophages from mice in which corresponding nucleotides encoding the amino acid at position 254 of FAMIN were edited. Collectively, these results identified the non-synonymous SNP rs3764147 that encodes FAMIN(p.I254V) as the causal genetic variation of this 'risk haplotype'.

Control of bactericidal and inflammasome activity by FAMIN

Finally, we turned our attention to the consequences of the profound metabolic derangement described above on immunological function. mROS can directly augment the bactericidal activity of macrophages directed against intracellular pathogens[29]. m*Famin*$^{-/-}$ M0 macrophages exhibited significantly less intracellular killing of a luminescent *Mycobacterium bovis* bacillus Calmette-Guérin (BCG) strain[30] than that of m*Famin*$^{+/+}$ M0 macrophages (**Fig. 7a**). Silencing *FAMIN* in human macrophages resulted in diminished bactericidal activity toward luminescent *M. bovis* BCG (**Fig. 7b**), similar to results obtained for mouse macrophages. Finally, more *Salmonella enterica* serovar Typhimurium were recovered from infected m*Famin*$^{-/-}$ M0 macrophages than from infected m*Famin*$^{+/+}$ M0 macrophages regardless of whether exogenous lipids were provided in serum or not (**Fig. 7c**); these results collectively demonstrated that FAMIN determined the capacity of macrophages to kill intracellular pathogens.

mROS also have a critical role in the caspase-1-mediated maturation of interleukin 1β (IL-1β) by the NLRP3 inflammasome[31]. The inflammasome assembles on mitochondria-associated membranes after triggering of cells by pathogen-associated molecular patterns[31]. The activation of m*Famin*$^{-/-}$ M1 macrophages by the NLRP3 inflammasome via treatment with lipopolysaccharide (LPS) plus ATP resulted in lower levels of cleaved active (p20) caspase-1 than those in m*Famin*$^{+/+}$ cells activated similarly. Consequently, there was barely detectable cleaved (p17) IL-1β in the lysates and supernatants of m*Famin*$^{-/-}$ M1 macrophages, in contrast to the readily detectable IL-1β in m*Famin*$^{+/+}$ M1 macrophages (**Fig. 7d**). Together these results demonstrated that FAMIN determined the capacity for triggering the NLRP3 inflammasome in M1 macrophages for secretion of the host innate danger signal IL-1β. Moreover, FAMIN-dependent inflammasome activation required intact FAO, as inhibition of FAO

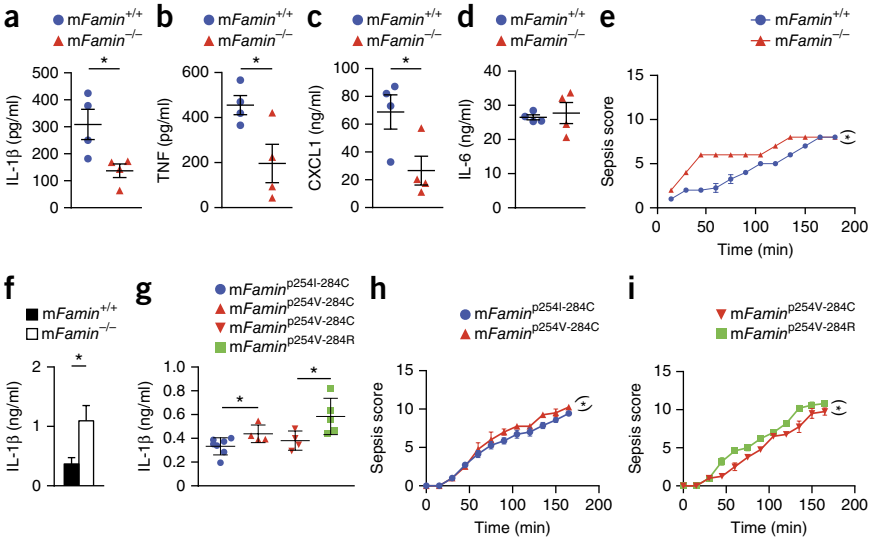

Figure 8 FAMIN deficiency causes dysregulated response to endotoxin *in vivo*. (**a**–**d**) Concentration of IL-1β (**a**), TNF (**b**), CXCL1 (**c**) and IL-6 (**d**) in serum from m*Famin*$^{+/+}$ and m*Famin*$^{-/-}$ mice 2 h after intraperitoneal injection of LPS (2 mg per kg body weight). (**e**,**f**) Clinical scores for sepsis severity (maximum score, 15) (**e**) and concentration of IL-1β in serum (**f**) of m*Famin*$^{+/+}$ and m*Famin*$^{-/-}$ mice 3 h after intraperitoneal injection of LPS (10 mg per kg body weight). (**g**) Concentration of IL-1β in 5-week-old homozygous m*Famin*$^{p254I-284C}$ mice and their homozygous m*Famin*$^{p254V-284C}$ control littermates or homozygous m*Famin*$^{p254V-284R}$ mice and their homozygous m*Famin*$^{p254V-284C}$ control littermates (key) treated as in **e**,**f**. (**h**,**i**) Clinical scores of sepsis severity (as in **e**) in m*Famin*$^{p254I-284C}$ and m*Famin*$^{p254V-284C}$ littermates (**h**) or m*Famin*$^{p254V-284R}$ and m*Famin*$^{p254V-284C}$ littermates (**i**) treated as in **e**,**f**. Each symbol (**a**–**d**,**g**) represents an individual mouse; small horizontal lines indicate the mean (± s.e.m.). $*P < 0.05$ and $**P < 0.01$ (Unpaired, two-tailed Student's *t*-test (**a**–**d**,**f**,**g**) or linear mixed model (**e**,**h**,**i**)). Data are from one experiment with four mice per group (**a**–**d**), three mice per group (**e**,**f**; mean ± s.e.m.) or seven mice (m*Famin*$^{p254I-284C}$), four mice (m*Famin*$^{p254V-284C}$ or m*Famin*$^{p254V-284C}$) or five mice (m*Famin*$^{p254V-284R}$) (**g**–**i**; mean ± s.e.m.).

with etomoxir in m*Famin*$^{+/+}$ M1 macrophages stimulated with LPS plus ATP resulted in less secretion of cleaved IL-1βp17 (**Fig. 7e**), similar to results obtained for zymosan-stimulated M1 macrophages (**Fig. 7f**); no additive effect of the inhibition of FAO was observed for m*Famin*$^{-/-}$ M1 macrophages (**Fig. 7e**). A similar pattern of FAO-dependent regulation was observed in LPS-stimulated M1 macrophages for the cytokine TNF and the chemokine CXCL1, while IL-6 secretion remained unaffected (**Fig. 7g–i**). Notably, intraperitoneal injection of LPS (2 mg per kg body weight) resulted in lower concentrations of IL-1β, CXCL1 and TNF in serum from m*Famin*$^{-/-}$ mice than in that from m*Famin*$^{+/+}$ mice, while the concentration of IL-6 remained unaffected (**Fig. 8a–d**). Notably, this pattern of LPS-induced regulation of serum cytokines is reminiscent of the inhibition of glycolysis *in vivo* with 2-deoxyglucose[11].

After being stimulated with LPS or with LPS plus ATP *in vitro*, mononuclear cells from patients with sJIA exhibit much less secretion of IL-1β than do cells from healthy donors, although it has remained unclear whether this is cause or consequence of active disease or is related to therapeutics[32]. Given that the rare SNP variant resulting in the substitution FAMIN(p.C284R) is the only firmly established genetic cause of sJIA so far[1,33], impaired induction of IL-1β upon stimulation with LPS and ATP *in vitro* would be consistent with our results obtained for m*Famin*$^{-/-}$ M1 macrophages. Nonetheless, blockade of IL-1 is therapeutic in the vast majority of patients with sJIA and leads to swift normalization of their fever, rash and acute-phase reactants[32,34,35]. We therefore hypothesized that the profound impairment in 'energetic reserves' in the absence of FAMIN function (reflected by low ATP and phosphocreatine, mitochondrial injury, and diminished FAO and glycolysis) might limit an organism's capacity to withstand serious injury. We injected a high dose of LPS (10 mg per kg body weight) intraperitoneally into m*Famin*$^{+/+}$ and m*Famin*$^{-/-}$ mice and continuously assessed the mice for clinical signs of sepsis over a 3-hour period. m*Famin*$^{-/-}$ mice had higher sepsis scores than those of m*Famin*$^{+/+}$ mice, and these findings were particularly apparent during the first 90 min of observation (**Fig. 8e**). Moreover, two of seven m*Famin*$^{-/-}$ mice also showed signs of epistaxis (consistent with a bleeding disorder), a feature not observed in m*Famin*$^{+/+}$ mice (data not shown). The higher sepsis scores of m*Famin*$^{-/-}$ mice were accompanied by a twofold higher concentration of IL-1β in serum from m*Famin*$^{-/-}$ mice than in that of m*Famin*$^{+/+}$ mice at the conclusion of the experiment (**Fig. 8f**). In analysis of 'SNP-mutant' mice, treatment with LPS (at a dose of 10 mg per kg body weight) resulted in the highest concentration of IL-1β in serum from m*Famin*$^{p254V-284R}$ mice, an intermediate concentration in m*Famin*$^{p254V-284C}$ mice and the lowest concentration in m*Famin*$^{p254I-284C}$ mice (**Fig. 8g**). Correspondingly, m*Famin*$^{p254V-284R}$ mice had higher clinical sepsis scores than those of m*Famin*$^{p254V-284C}$ mice, and m*Famin*$^{p254V-284C}$ mice had higher clinical sepsis scores than those of m*Famin*$^{p254I-284C}$ mice (**Fig. 8h**,**i**). Collectively, these results demonstrated that in the absence of FAMIN function, a high dose of LPS led to catastrophic activation of IL-1β. We speculate that the impaired bioenergetic reserves of m*Famin*$^{-/-}$ mice might tip the balance of sepsis-associated inflammasome activation toward a pyroptotic, pro-death response, as has been reported in other contexts[36].

DISCUSSION

At the level of the organism, FAO and glucose oxidation are reciprocal metabolic pathways referred to as 'the Randle cycle'[37]. Similarly, coupling of DNL and FAO is not energetically efficient in terms of ATP production but nonetheless are engaged in certain immune and non-immune cells[38–40]. In macrophages, FAMIN promotes flux through DNL to concomitantly drive high levels of both FAO and glycolysis. FAMIN thereby profoundly determines the maximum bioenergetic capacity of macrophages. The closest orthologs of FAMIN belong to a new class of proteins (the DUF152 ('domain of unknown function 152') family), and those with a reported function are bacterial proteins that exhibit atypical laccase (phenol-oxidoreductase) activity[41,42]. We purified recombinant eukaryotically expressed human FAMIN(p.254I) and FAMIN(p.254V) and did not observe any laccase activity toward a series of prototypical substrates (data not shown). At this stage, the precise biochemical mechanism whereby FAMIN enhances DNL-dependent FAO remains unclear.

Intriguingly, FAMIN-dependent FAO occurred even when it was uncoupled from ATP synthesis, as in M1 macrophages, and might be of greatest importance in this setting for supporting glycolysis. 'Uncoupled' FAO has been suggested to have a critical role in cancer

cells engaged in aerobic glycolysis[43]. Moreover, inhibition of DNL at the level of the acetyl-CoA carboxylase ACC1 (the enzyme that synthesizes the malonyl-CoA required for FASN function) has been reported to impair glycolysis in helper T cells[44]. Here we identified a critical role for FAO in M1 macrophages that was required for IL-1β activation and ROS production. Glycolysis in M1 macrophages is well known to be critically required for IL-1β production[11]. In contrast, the importance of β-oxidation has received less attention, even though FAO, not glycolysis, has been reported to be the sole driver of bactericidal mROS production in *Salmonella*-infected macrophages[45]. Moreover, FAMIN-dependent mROS production also determines the maximal capacity of the NADPH oxidase system, the main source of bactericidal ROS in M1 macrophages.

While metabolic pathways in immune cells are emerging as important determinants of immunological function[46], we found here that a core metabolic regulator in immune cells was affected by genetic variation that results in a predisposition for inflammatory diseases and infection. Patients with systemic JIA, a condition demonstrated here as arising from a defect at the peroxisome–mitochondria interface, present with a characteristic daily (quotidian) spiking fever[33]. Deficiency in mevalonate kinase, a peroxisomal enzyme involved in cholesterol biosynthesis, causes hyper-IgD syndrome, a related juvenile periodic fever[47]. Remarkably, the mevalonate pathway has a precursor common with that of DNL, cytosolic acetyl-CoA, which raises the possibility of commonality in mechanism. Intriguingly, both sJIA and hyper-IgD syndrome seem to be triggered by childhood infections or vaccinations[33,47]. Diversity in such environmental triggers might also explain how homozygosity for the loss-of-function FAMIN variant p.C284R can result in two very different diseases, sJIA and early-onset CD[1,2], an aspect even more pertinent for the FAMIN variant p.I254V, which results in a predisposition for CD.

In summary, we found here that FAMIN controlled acyl-CoA synthesis through DNL at peroxisomes and thereby fed FAO and regulated glycolysis. This has profound implications for cellular energy homeostasis and immunological function in organisms, with hypomorphy promoting autoinflammation.

METHODS

Methods and any associated references are available in the online version of the paper.

Note: Any Supplementary Information and Source Data files are available in the online version of the paper.

ACKNOWLEDGMENTS

We thank G. Brown for help with laccase assays; J. Murkin and M. Deery for proteomics; L. Porter for metabolic-flux assays; J. Skepper for electron microscopy; I. Purvis for help with *in vivo* procedures; R. Rodrigues, M. Md-Ibrahim and J. Jones for cellular assays; S. Dhillon for the generation of constructs; T. Lawley, M. Pardo, J. Choudhary, K. Smith, J. Lee, D. Thomas, G. Schneditz, L. Haag, M. Parkes and R. Blumberg for discussions; all National Institute for Health Research Cambridge BioResource volunteers for the participation; the Cambridge BioResource staff for help with volunteer recruitment; members of the Cambridge BioResource SAB and Management Committee for support of this study; and the National Institute for Health Research Cambridge BRC Cell Phenotyping Hub for expertise and help. Access to Cambridge BioResource volunteers and their data and samples is governed by the Cambridge BioResource SAB (documents on access arrangements and contact details, http://www.cambridgebioresource.org.uk/). Supported by the European Research Council under the European Community's Seventh Framework Programme (FP7/2007-2013)/ERC Grant agreement 260961 (A.K.), the Wellcome Trust (investigator award 106260/Z/14/Z to A.K.; a PhD fellowship for clinicians to M.Z.C.; and a Career Re-Entry Fellowship to N.C.K.), the Wellcome Trust Sanger Institute (G.D., A.B., S.M., S.C. and K.B.), the US National Institutes of Health (5U420D011174 and 5U54HG006348 to A.B. and K.B.), the Biotechnology and Biological Sciences Research Council (M.J.O.W.), the National Institute for Health Research Cambridge Biomedical Research Centre, the European Crohn's and Colitis Organisation (M.T.) and the Swedish Medical Research Council and the Olle Engkvist foundation (M.D'A.).

AUTHOR CONTRIBUTIONS

M.Z.C., together with S.L.K., G.W.S., S.S., J.W.A., M.T., T.R. and N.C.K., designed and performed most of the experiments; K.B., B.D. and A.B. designed, generated and confirmed the genotype of CRISPR-Cas9–generated mouse lines; Q.Z. and M.J.O.W. provided lipidomics experiments and analysis; G.A. and M.D'A. identified the cellular localization of FAMIN; S.C., S.M. and G.D. contributed *Salmonella* and part of the *in vivo* experimentation; K.P.B. and R.A.F. contributed to mycobacterial experiments; E.R.C. helped with metabolic-flux assays and ROS experimentation; J.L.G. contributed metabolomics experimentation and analysis; and A.K. devised and coordinated the project and, together with M.Z.C. and G.D., and with contributions from all authors, designed experiments, interpreted data and wrote the manuscript.

COMPETING FINANCIAL INTERESTS

The authors declare no competing financial interests.

1. Wakil, S.M. *et al.* Association of a mutation in LACC1 with a monogenic form of systemic juvenile idiopathic arthritis. *Arthritis Rheumatol.* **67**, 288–295 (2015).
2. Patel, N. *et al.* Study of Mendelian forms of Crohn's disease in Saudi Arabia reveals novel risk loci and alleles. *Gut* **63**, 1831–1832 (2014).
3. Liu, H. *et al.* Discovery of six new susceptibility loci and analysis of pleiotropic effects in leprosy. *Nat. Genet.* **47**, 267–271 (2015).
4. Jostins, L. *et al.* Host-microbe interactions have shaped the genetic architecture of inflammatory bowel disease. *Nature* **491**, 119–124 (2012).
5. Hruz, T. *et al.* Genevestigator v3: a reference expression database for the meta-analysis of transcriptomes. *Adv. Bioinformatics* **2008**, 420747 (2008).
6. Heng, T.S. & Painter, M.W. The Immunological Genome Project: networks of gene expression in immune cells. *Nat. Immunol.* **9**, 1091–1094 (2008).
7. Jensen-Urstad, A.P. & Semenkovich, C.F. Fatty acid synthase and liver triglyceride metabolism: housekeeper or messenger? *Biochim. Biophys. Acta* **1821**, 747–753 (2012).
8. Jensen-Urstad, A.P. *et al.* Nutrient-dependent phosphorylation channels lipid synthesis to regulate PPARα. *J. Lipid Res.* **54**, 1848–1859 (2013).
9. Lodhi, I.J. & Semenkovich, C.F. Peroxisomes: a nexus for lipid metabolism and cellular signaling. *Cell Metab.* **19**, 380–392 (2014).
10. Murray, P.J. *et al.* Macrophage activation and polarization: nomenclature and experimental guidelines. *Immunity* **41**, 14–20 (2014).
11. Tannahill, G.M. *et al.* Succinate is an inflammatory signal that induces IL-1β through HIF-1α. *Nature* **496**, 238–242 (2013).
12. Huang, S.C. *et al.* Cell-intrinsic lysosomal lipolysis is essential for alternative activation of macrophages. *Nat. Immunol.* **15**, 846–855 (2014).
13. Skarnes, W.C. *et al.* A conditional knockout resource for the genome-wide study of mouse gene function. *Nature* **474**, 337–342 (2011).
14. Hillebrand, M. *et al.* Identification of a new fatty acid synthesis-transport machinery at the peroxisomal membrane. *J. Biol. Chem.* **287**, 210–221 (2012).
15. Semenkovich, C.F. Regulation of fatty acid synthase (FAS). *Prog. Lipid Res.* **36**, 43–53 (1997).
16. Jha, A.K. *et al.* Network integration of parallel metabolic and transcriptional data reveals metabolic modules that regulate macrophage polarization. *Immunity* **42**, 419–430 (2015).
17. Grevengoed, T.J., Klett, E.L. & Coleman, R.A. Acyl-CoA metabolism and partitioning. *Annu. Rev. Nutr.* **34**, 1–30 (2014).
18. Carracedo, A., Cantley, L.C. & Pandolfi, P.P. Cancer metabolism: fatty acid oxidation in the limelight. *Nat. Rev. Cancer* **13**, 227–232 (2013).
19. Wu, M. *et al.* Multiparameter metabolic analysis reveals a close link between attenuated mitochondrial bioenergetic function and enhanced glycolysis dependency in human tumor cells. *Am. J. Physiol. Cell Physiol.* **292**, C125–C136 (2007).
20. Hao, W., Chang, C.P., Tsao, C.C. & Xu, J. Oligomycin-induced bioenergetic adaptation in cancer cells with heterogeneous bioenergetic organization. *J. Biol. Chem.* **285**, 12647–12654 (2010).
21. Newsholme, E.A., Sugden, P.H. & Williams, T. Effect of citrate on the activities of 6-phosphofructokinase from nervous and muscle tissues from different animals and its relationships to the regulation of glycolysis. *Biochem. J.* **166**, 123–129 (1977).
22. Fantin, V.R., St-Pierre, J. & Leder, P. Attenuation of LDH-A expression uncovers a link between glycolysis, mitochondrial physiology, and tumor maintenance. *Cancer Cell* **9**, 425–434 (2006).
23. Vats, D. *et al.* Oxidative metabolism and PGC-1β attenuate macrophage-mediated inflammation. *Cell Metab.* **4**, 13–24 (2006).
24. Landree, L.E. *et al.* C75, a fatty acid synthase inhibitor, modulates AMP-activated protein kinase to alter neuronal energy metabolism. *J. Biol. Chem.* **279**, 3817–3827 (2004).
25. Liesa, M. & Shirihai, O.S. Mitochondrial dynamics in the regulation of nutrient utilization and energy expenditure. *Cell Metab.* **17**, 491–506 (2013).

26. Murphy, M.P. How mitochondria produce reactive oxygen species. *Biochem. J.* **417**, 1–13 (2009).
27. Yu, L., Quinn, M.T., Cross, A.R. & Dinauer, M.C. $gp91^{phox}$ is the heme binding subunit of the superoxide-generating NADPH oxidase. *Proc. Natl. Acad. Sci. USA* **95**, 7993–7998 (1998).
28. Ran, F.A. *et al.* Genome engineering using the CRISPR-Cas9 system. *Nat. Protoc.* **8**, 2281–2308 (2013).
29. West, A.P. *et al.* TLR signalling augments macrophage bactericidal activity through mitochondrial ROS. *Nature* **472**, 476–480 (2011).
30. Kampmann, B. *et al.* Evaluation of human antimycobacterial immunity using recombinant reporter mycobacteria. *J. Infect. Dis.* **182**, 895–901 (2000).
31. Zhou, R., Yazdi, A.S., Menu, P. & Tschopp, J. A role for mitochondria in NLRP3 inflammasome activation. *Nature* **469**, 221–225 (2011).
32. Gattorno, M. *et al.* The pattern of response to anti-interleukin-1 treatment distinguishes two subsets of patients with systemic-onset juvenile idiopathic arthritis. *Arthritis Rheum.* **58**, 1505–1515 (2008).
33. Mellins, E.D., Macaubas, C. & Grom, A.A. Pathogenesis of systemic juvenile idiopathic arthritis: some answers, more questions. *Nat. Rev. Rheumatol.* **7**, 416–426 (2011).
34. Quartier, P. *et al.* A multicentre, randomised, double-blind, placebo-controlled trial with the interleukin-1 receptor antagonist anakinra in patients with systemic-onset juvenile idiopathic arthritis (ANAJIS trial). *Ann. Rheum. Dis.* **70**, 747–754 (2011).
35. Pascual, V., Allantaz, F., Arce, E., Punaro, M. & Banchereau, J. Role of interleukin-1 (IL-1) in the pathogenesis of systemic onset juvenile idiopathic arthritis and clinical response to IL-1 blockade. *J. Exp. Med.* **201**, 1479–1486 (2005).
36. Leist, M., Single, B., Castoldi, A.F., Kühnle, S. & Nicotera, P. Intracellular adenosine triphosphate (ATP) concentration: a switch in the decision between apoptosis and necrosis. *J. Exp. Med.* **185**, 1481–1486 (1997).
37. Hue, L. & Taegtmeyer, H. The Randle cycle revisited: a new head for an old hat. *Am. J. Physiol. Endocrinol. Metab.* **297**, E578–E591 (2009).
38. Guan, H.P. *et al.* A futile metabolic cycle activated in adipocytes by antidiabetic agents. *Nat. Med.* **8**, 1122–1128 (2002).
39. O'Sullivan, D. *et al.* Memory $CD8^+$ T cells use cell-intrinsic lipolysis to support the metabolic programming necessary for development. *Immunity* **41**, 75–88 (2014).
40. van der Windt, G.J. *et al.* CD8 memory T cells have a bioenergetic advantage that underlies their rapid recall ability. *Proc. Natl. Acad. Sci. USA* **110**, 14336–14341 (2013).
41. Beloqui, A. *et al.* Novel polyphenol oxidase mined from a metagenome expression library of bovine rumen: biochemical properties, structural analysis, and phylogenetic relationships. *J. Biol. Chem.* **281**, 22933–22942 (2006).
42. Kim, Y. *et al.* Crystal structure of hypothetical protein YfiH from *Shigella flexneri* at 2 A resolution. *Proteins* **63**, 1097–1101 (2006).
43. Samudio, I. *et al.* Pharmacologic inhibition of fatty acid oxidation sensitizes human leukemia cells to apoptosis induction. *J. Clin. Invest.* **120**, 142–156 (2010).
44. Berod, L. *et al. De novo* fatty acid synthesis controls the fate between regulatory T and T helper 17 cells. *Nat. Med.* **20**, 1327–1333 (2014).
45. Hall, C.J. *et al.* Immunoresponsive gene 1 augments bactericidal activity of macrophage-lineage cells by regulating β-oxidation-dependent mitochondrial ROS production. *Cell Metab.* **18**, 265–278 (2013).
46. O'Neill, L.A. & Pearce, E.J. Immunometabolism governs dendritic cell and macrophage function. *J. Exp. Med.* **213**, 15–23 (2016).
47. Mulders-Manders, C.M. & Simon, A. Hyper-IgD syndrome/mevalonate kinase deficiency: what is new? *Semin. Immunopathol.* **37**, 371–376 (2015).

ONLINE METHODS

Mice. Ear-biopsy genomic DNA was used for routine genotyping of all mice. Primer sequences are shown in **Supplementary Table 3**. C57BL/6N mice were bred and maintained in specific pathogen-free conditions at the Central Biomedical Services (CBS) facility, University of Cambridge and at the Wellcome Trust Sanger Institute. All procedures performed in studies involving animals were in accordance with the ethical standards of the institution or practice at which the studies were conducted, and all were conducted with approval of the UK home office. m*Famin*$^{-/-}$, m*Famin*^{p284R} and m*Famin*^{p254I} mice generated as described below littered at Mendelian ratios and developed normally and no spontaneous disease emerged under specific pathogen free (SPF) conditions. Six- to twelve-week-old mice that were age and sex matched as described in the relevant methods sections were used for all experiments unless otherwise stated.

m*Famin*$^{-}$ allele. m*Famin*$^{-/-}$ mice were generated by disruption of the mouse homolog (*9030625A04Rik*; *Lacc1*) of human *C13orf31* (*LACC1*) by homologous recombination in C57BL/6N-A/a embryonic stem (ES) cells (**Supplementary Fig. 3**) to generate mice on a pure C57BL/6NTac background (ES cell clone ID EPD0538_1_D06 (International Knockout Mouse Consortium))[13].

CRISPR-Cas9 target sites and vector construction. CRISPR target sites were identified using the CRISPR design website (http://crispr.mit.edu/) as described[28] and are shown in **Supplementary Table 4**. The strategy to generate mouse lines carrying the p.254I and p.284R FAMIN variants (corresponding residue numbers are identical for human *C13orf31* and mouse *9030625A04Rik*) is shown in **Supplementary Figure 3**. In brief, wild-type C57BL/6NTac mice carry p.254V (human 'risk' variant) and p.284C. For introduction of the 'non-risk' p.254I allele, guide RNA (gRNA) 'line7' along 'oligo 7' or 'oligo 7 wobble' were used, the latter introducing two additional synonymous nucleotide changes (**Supplementary Table 4** and **Supplementary Fig. 3**). The corresponding strategy for introduction of the 'Mendelian variant' p.284R with gRNA 'line9' along 'oligo 9' or 'oligo 9 wobble' is shown in **Supplementary Figure 3**. Oligonucleotide tyrex2R (**Supplementary Table 4**) was co-injected with each of the four lines to target the *Tyr* gene to allow color-based selection. The selected gRNA sequences were cloned into a gRNA vector containing the gRNA backbone and a T7 promoter to facilitate RNA production (BsaI sites). Cas9 mRNA was produced using a previously described vector modified to contain a T7 promoter[48]. The integrity of all plasmids was confirmed by DNA sequencing. The targeting oligonucleotides were synthesized as desalted ssDNA oligonucleotides from Integrated DNA Technologies (IDT).

Cas9 and gRNA production. For Cas9 RNA production, the T7/Cas9 plasmid was linearized (EcoRI), purified with PCR purification kit (Qiagen) and *in vitro* transcribed using mMessage mMachine T7 Ultra kit (Life Technologies). For gRNA production, the plasmid was linearized (DraI), purified with PCR purification kit (Qiagen) and *in vitro* transcribed using the MEGAshortscript T7 kit (Life Technologies). Both Cas9 mRNA and gRNA were purified using the MEGAclear kit (Life Technologies) and were eluted in RNase-free water. The quality of the RNA was analyzed using Agilent RNA 6000 Nano kit (Agilent Technologies, 2100 Bioanalyzer) and Qubit RNA BR assay kit (Thermo Fisher Scientific).

One-cell embryo injection. Twelve 4- to 5-week old C57BL/6NTac females were super-ovulated by intraperitoneal injection of 5 IU of pregnant mare's serum (PMSG) at 12:00-13:00 h (on a 12 h light/dark cycle, on at 07:00/off at 19:00) followed 48 h later by an intraperitoneal injection of 5 IU human chorionic gonadotrophin (hCG) and were mated overnight with C57BL/6NTac stud males. The next morning the females were checked for the presence of a vaginal copulation plug as evidence of successful mating, and oviducts were dissected at approximately 21–22 h post hCG. Cumulus masses from these were released and treated with hyaluronidase, and the fertilized one-cell embryos were left in KSOM media ready for cytoplasmic injection, as previously described[49]. 50 ng/µl Cas9 mRNA, 25 ng/µl gRNA and 100 ng/µl oligonucleotide were mixed in RNase-free water and injected into the cytoplasm of fertilized one-cell embryos in FHM medium. One-cell injected embryos were transferred the same day by oviductal embryo transfer into 0.5 d post-coital pseudo-pregnant female BJCB strain (CBA<Wtsi>;C57BL/6J-Jax F1) recipients, produced by estrus selection and overnight mating to vasectomized males[49].

Cytoplasmic injection. Injections were performed using a new cytoplasmic injection technique. An injector using a positive balance pressure, such as an Eppendorf Femtojet, was connected to a microinjection tip filled with the CRISPR materials. The microinjection tip was steadily advanced toward the opposite side of the zygote, which was anchored by the holding pipette until the micropipette passed through the plasma membrane to break it. The pipette was then drawn back into the cytoplasm, the CRISPR mix was delivered and the micropipette was immediately withdrawn. A successful injection was indicated by visible movement in the cytoplasm.

SNP-mutant-mice breeding strategy. Illumina sequencing of the m*Famin* gene was used in founder and F1 generation mice, confirmed by Sanger sequencing, to assess for successful gene editing. Founder mice were crossed with wild-type C57BL/6NTac mice to generate m*Famin*$^{p254I/p254V}$ and m*Famin*$^{p284R/p284C}$ heterozygous mice, which were then intercrossed, and homozygous littermates were used for experiments. Mice generated with and without wobble bases in targeting oligonucleotides were maintained separately and were used in experiments alongside their littermate controls irrespective of the presence or absence of wobble bases. Offspring from several founders were used to populate genotype categories in experiments. Routine genotyping was performed via Sanger sequencing.

Genotype-selected human samples. Peripheral blood for human neutrophil and monocyte isolation was collected from healthy volunteers from a genotype-selectable bioresource of ~10,000 donors (Cambridge BioResource; http://www.cambridgebioresource.org.uk). Healthy age- and sex-matched donors identified as homozygous for the 'risk haplotype' (G/G) or 'non-risk haplotype' (A/A) at SNP rs3764147, encoding FAMIN(p.254V) and FAMIN(p.254I) respectively, were recruited to participate in the study. Nucleotide positions in text correspond to genome assembly GRCh38.p2. None of the volunteers had received corticosteroid or immunosuppressant therapy within 6 months of enrollment. Investigators were kept blinded to the genotype of samples until study completion, with all individual experimental procedures performed on ('blinded') genotype pairs. The study protocol has been reviewed and approved by the South Central Berkshire B Research Ethics Committee (15/SC/0068), and written informed consent was obtained from each subject.

Antibodies and reagents. The following antibodies were used for immunoblotting. Abcam: anti-PMP70 (1:1,000 dilution; ab3421), anti-FASN (1µg/ml dilution; ab22759); Cell Signaling: anti-cytochrome oxidase IV (1:250 dilution; 4850), anti-catalase (1:800 dilution; 12980), anti-centromere protein A (1:400 dilution; 2186), anti-calreticulin (1:200 dilution; 12238), anti-FASN (1:1,000 dilution; 3180); Santa Cruz Biotechnology: anti-C13orf31 (anti-FAMIN) (1:200 dilution; sc-374553; E7 and 1:500 dilution; sc-376231; E12), anti-caspase 1 p20 (1:250 dilution; sc-1218-R); R&D Systems: anti-IL-1β (1:250 dilution; AF-401-NA); Sigma: anti-β-actin (1:10,000 dilution; A5060). All antibodies used have validation profiles on either Antibodypedia or 1DegreeBio.

The following reagents were used: M-CSF (Peprotech, 300-25), LPS (from *Escherichia coli* K12, InvivoGen, tlrl-peklps), human IFN-γ (Peprotech, 300-02), mouse IFN-γ (Peprotech, 315-05), human IL-4 (Peprotech, 200-04), mouse IL-4 (Peprotech, 214-14), ATP (Sigma-Aldrich, A2383), C75 (Sigma-Aldrich, C5490), etomoxir (Sigma-Aldrich, E1905), MitoTEMPO (Sigma-Aldrich, SML0737), oligomycin (Sigma-Aldrich, O4876), FCCP (Sigma-Aldrich, C2920), rotenone (Sigma-Aldrich, R8875), antimycin A (Sigma-Aldrich, A8674), palmitate-BSA (Seahorse Bioscience, 102720-100), zymosan A (Sigma-Aldrich, Z4250), PMA (Sigma-Aldrich, P1585), HRP (Sigma-Aldrich, P8375), luminol (Sigma-Aldrich, A8511).

Mouse bone-marrow-derived macrophages and neutrophils. Bone marrow was flushed from mouse femurs and tibias, filtered through a 70 µm cell strainer and incubated in complete medium (RPMI-1640 containing 100 U/ml of penicillin-streptomycin, 1 mM HEPES pH 7.4) and 10% FBS. Bone-marrow-derived macrophages (BMDMs) were prepared by culturing cells for 6 d in the presence of 100 ng/ml of M-CSF. After harvesting and

re-seeding, macrophages were polarized for 16 h toward M1 or M2 with IFN-γ (50 ng/ml) plus LPS (20 ng/ml) or with IL-4 (20 ng/ml), respectively, and where indicated, in the presence or absence of C75 (20 μM) and etomoxir (100 μM). Bone-marrow neutrophils were prepared using a neutrophil isolation kit (Miltenyi Biotec) according to the manufacturer's instructions.

Human peripheral-blood-derived macrophages. For studies of human cells, blood received from healthy donors was used to isolate peripheral blood mononuclear cells and neutrophils by Lymphoprep (Axis-Shield) gradient centrifugation. Monocyte-derived macrophages were generated by resuspending cells in complete RPMI-1640 and plated on Nunclon surface tissue culture dishes (Nunc). After 2 h, non-adherent cells were discarded and the remaining monocytes cultured for 4 d in complete medium with 10% FBS and 40 ng/ml M-CSF. At day 4, macrophages were harvested and polarized into M1 and M2 as described for mouse macrophages. Neutrophils were concurrently isolated during Lymphoprep gradient centrifugation (Axis-Shield) by sedimentation of the red blood cell–neutrophil layer with 10% dextran, followed by hypotonic lysis of contaminating erythrocytes.

Cell lines. THP-1 and U937 cell lines were maintained in complete RPMI-1640 with 10% FBS. To polarize into M1 macrophages, cells were incubated overnight with 50 ng/ml IFN-γ plus 20 ng/ml LPS and for M2 macrophages, cells were treated with 1 μM of PMA for 6 h and then polarized with 50 ng/ml IL-4 and 50 ng/ml IL-13. HEK293 and HEK293T cells were maintained in DMEM with 10% FBS. All cell lines were purchase from ATCC, which guarantees cell-line authentication.

Plasmids. The gene encoding human FAMIN (*C13orf31* (*LACC1*); called '*FAMIN*' below) was amplified from an IMAGE clone (MHS1010-7508636) using a forward primer containing a KpnI site followed by a Kozak sequence and start codon and reverse primer containing a BamHI site, excluding the stop codon of FAMIN and was cloned into KpnI and BamHI digested and dephosphorylated pEXPR-IBA103 (IBA Life Sciences) to generate C-terminal Strep III tag FAMIN. The same IMAGE clone was amplified with a forward primer containing a SacII site and a reverse primer containing an XhoI site and cloned into pEXPR-IBA105 to generate *N*-terminal Strep III tag *FAMIN*. Strep-tag III is a sequential arrangement of two Strep-tag II sequences (Trp-Ser-His-Pro-Gln-Phe-Glu-Lys) separated by a short linker. Constructs were sequence verified, with Strep-tag III in-frame with FAMIN. *FAMIN* containing a stop codon was also cloned into pEXPR-IBA103 for use as an untagged FAMIN control.

FAMIN variants were introduced by site-directed mutagenesis (Agilent Quick change II XL SDM kit) using the above constructs as template. To introduce the p.254V substitution, the following primers were used: Forward, 5′-AGACTCATCATTCCAATGACGTCTGGATTATGGGAAGAAAG-3′; Reverse, 5′-TAAAGACTCATCATTCCAATGACATCTGGATTATGGGAAGAAAGGAG-3′ and to introduce the p.284R mutation the following primers were used: Forward, 5′-CAAAAACTATCGGTATACGGTCTGCACCAAGAGCTGC-3′; Reverse 5′-GCAGCTCTTGGTGCAGACCGTATACCGATAGTTTTTG-3′. All constructs were sequence verified in both forward and reverse orientations.

Protein affinity-purification mass spectrometry. HEK293T cells were transfected with pEXPR-IBA103 vector only or plasmid constructs encoding untagged FAMIN, N-terminal Strep-tag FAMIN or C-terminal Strep-tag FAMIN using Lipofectamine 2000 (Invitrogen) following the manufacturer's instructions. 48 h following transfection, cells were washed twice in ice-cold PBS and harvested by gently scraping into 5 ml ice-cold lysis buffer containing 20 mM HEPES-KOH, pH 7.5, 150 mM KCl, 1% Nonidet P-40, 0.1 mM phenylmethylsulfonyl fluoride, and protease inhibitor mixture. Cells were incubated on ice for 10 min, then were homogenized by shearing 20 times through a 21-gauge needle. The protein lysate was centrifuged for 15 min at 4 °C at 3,000*g* and the protein supernatant was collected into a freshly chilled tube to remove cellular debris. 1 U/ml of avidin was added to block endogenous biotin and incubated on ice for 15 min and then re-centrifuged for a further 10 min at 4 °C. Supernatant containing Strep-tag labeled FAMIN protein was precipitated using a Strep-Tactin column (IBA Life Sciences). Strep-tagged FAMIN protein complexes were eluted using 2.5 mM desthiobiotin and eluted fractions were subjected to SDS-PAGE separation, followed by silver staining or immunoblot analysis. Gels were submitted to the Cambridge Centre for Proteomics, Department of Biochemistry and were excised manually. Proteins were reduced, carboxyamide methylated, and then digested to peptides using trypsin on a MassPrepStation (Micromass). The resulting peptides were applied to liquid chromatography coupled with tandem mass spectrometry (LC-MS/MS) on a QTof (Micromass). Fragmentation data were used to search the National Center for Biotechnology Information database using the MASCOT search engine (http://www.matrixscience.com).

Lipid mass spectrometry. Day-6 macrophages were seeded at 5×10^6 cells per 60 mm dish and polarized under M1 or M2 conditions. Cells were harvested, washed twice in ice-cold PBS and then flash-frozen in liquid nitrogen. For 1, 2-^{13}C-glucose–tracing experiments, macrophages were polarized overnight and then cultured for 24 h in the presence of 10 mM 1,2-^{13}C-glucose (Sigma). Cell pellets were washed twice with cold PBS and re-suspended in 1.5 ml methanol. After spiking with 40 μl lipid standards cocktail mix of 50 ng 17:0-FaCN, 100 ng 17:0-FaCoA and 400 ng 17:0-FFA, 1.5 ml of LCMS-grade water and 3 ml chloroform were added in. The mixture was subjected to Folch extraction. After collection of the lower phase, the upper phase was re-extracted with 3 ml synthetic lower phase (chloroform/methanol/water at volume ratio of 2:1:1, using the lower phase for re-extraction of lipid). The lower phase from both extractions was combined and dried under vacuum at 20 °C with SpeedVac (Thermo) and re-dissolved in 100 μl chloroform. 7 μl were injected for LC/MS/MS analysis. A Thermo Orbitrap Elite system (Thermo Fisher) hyphenated with a five-channel online degasser, four-pump, column oven, and autosampler with cooler Shimadzu Prominence HPLC system (Shimadzu) was used for lipid analysis. In detail, lipid classes were separated on a normal-phase Cogent silica-C column (150 × 2.1 mm, 4 μm, 100 Å, MicoSolv Technology) with hexane/dichloromethane/chloroform/methanol/acetanitrile/water/ethylamine solvent gradient based on the polarity of head group. High resolution (240k at m/z 400) / accurate mass (with mass accuracy <5 ppm) were used for molecular species identification and quantification. The identity of lipid was further confirmed by reference to appropriate lipids standards. Orbitrap Elite mass spectrometer operation conditions were as follows. For positive ion analysis: heated ESI source in positive ESI mode; heater temperature, 325 °C; sheath gas flow rate (arb), 35; aux gas flow rate (arb), 5; sweep gas flow rate (arb), 0; I spray voltage, 3.5 kV; capillary temperature, 325 °C; and S-lens RF level, 60%. Orbitrap mass analyzer was operated as SIM scan mode with two events. Event 1: mass range, *m/z* 238-663; and mass resolution, 240 k at *m/z* 400. Event 2: mass range, m/z 663-1088; and mass resolution, 240 k at *m/z* 400. B. For negative ion analysis, heated ESI source in negative ESI mode; heater temperature, 325 °C; sheath gas flow rate (arb), 45; aux gas flow rate (arb), 10; sweep gas flow rate (arb), 0; I spray voltage, 3.0 kV; capillary temperature, 375 °C; and S-lens RF Level, 70%. Orbitrap mass analyzer was operated as SIM scan mode with two events. Event 1: mass range, *m/z* 218-628; and mass resolution, 240 k at *m/z* 400. Event 2: mass range, *m/z* 628-1038; and mass resolution, 240 k at *m/z* 400. All the solvents used for lipids extraction and LC/MS/MS analysis are LC-MS grade from FisherScientific.

Aqueous metabolites mass spectrometry. Metabolites were extracted from 5×10^6 macrophages using methanol/chloroform. The organic and aqueous fractions were separated by the addition of water and chloroform. The aqueous layer was analyzed subsequently for metabolomics. Mass spectrometry was performed on an AB Sciex 5500 (Warrington) coupled to an Acquity ultra performance liquid chromatography (UPLC) system from Waters. For chromatography of Krebs-cycle intermediates, metabolites were separated on a BEH amide HILIC column (100 × 2.1 mm, 1.7 μm; Waters) in negative ion mode. After drying, the samples were analyzed on a HSS T3 column (100 × 2.1 mm, 1.7 μm; Waters). Cone voltage, collision energy and mass transitions were optimized for each metabolite for quantification. Data are presented in arbitrary units as the area ratio of metabolite peak relative to the internal standard.

ATP assay. ATP content in total cell lysates was measured using an ATP determination kit (Molecular probes, A22066). M1 and M2 macrophages were trypsinized after an overnight polarization and counted, and 2×10^5 cells were lysed in 100 mM Tris pH 7.75, 4 mM EDTA and 1% Triton-X.

doi:10.1038/ni.3532

Protein concentration was determined by BCA (Pierce, 23225). Remaining lysates were boiled at 96 °C, spun down for 1 min at 1,000*g* and the assay was performed according to the manufacturer's protocol. The amount of ATP was determined from the standard curve and is presented as nM of ATP per mg of protein in the sample.

NADPH quantification. NADPH concentration was determined using the NADP/NADPH Assay kit (Abcam, ab65349) according to the manufacturer's protocol. 4×10^6 macrophages were harvested in extraction buffer and filtered through a 10-kDa Spin column (Abcam, ab93349). The NADPH cycling reaction was performed for 2 h, and the NADPH amount was determined from the standard curve and normalized to protein concentration.

Oxygen-consumption rate and extracellular acidification rate. Macrophages were plated in XF-96 cell culture plates (7.5×10^5 cells/well) and polarized to M1 and M2 in the presence or absence of 20 μM C75 for 16 h. Macrophages were then washed and incubated for 1 h in XF assay medium (unbuffered DMEM pH 7.4 with 10 mM glucose and 2 mM L-glutamine, with or without 2 mM sodium pyruvate) in a non-CO_2 incubator at 37 °C as per manufacturer's instructions (Seahorse Bioscience). Real-time measurements of macrophage extracellular acidification rate (ECAR) and oxygen consumption rate (OCR) were performed using an XF-96 Extracellular Flux Analyzer (Seahorse Bioscience). Three or more consecutive measurements were obtained under basal conditions and after the sequential addition of 1 μM oligomycin, to inhibit mitochondrial ATP synthase; 1.5 μM FCCP (fluoro-carbonyl cyanide phenylhydrazone), a protonophore that uncouples ATP synthesis from oxygen consumption by the electron-transport chain; and 100 nM rotenone plus 1 μM antimycin A, which inhibits the electron transport chain. SRC is calculated as the difference between basal OCR and maximal OCR after the addition of FCCP. To assess glycolysis, three or more consecutive ECAR measurements were obtained under basal conditions and after the sequential addition of 1 μM oligomycin, to elicit maximal glycolytic capacity and 100 mM 2-DG (2-deoxyglucose) to inhibit glycolysis-dependent ECAR. Measurement of endogenous and exogenous fatty-acid oxidation (FAO) was performed according to the manufacturer's instructions (Seahorse Bioscience). In brief, macrophages were seeded and polarized toward M2 as above. After 16 h, macrophages were cultured in substrate limited DMEM medium containing 0.5 mM glucose, 1 mM GlutaMAX, 0.5 mM carnitine and 1% FBS for 24 h. Macrophages were then washed and incubated for 1 h in FAO assay medium (111 mM NaCl, 4.7 mM KCl, 1.25 mM $CaCl_2$, 2 mM $MgSO_4$, 1.2 mM NaH_2PO_4) supplemented with 2.5 mM glucose, 0.5 mM carnitine, and 5 mM HEPES, pH 7.4 in the presence or absence of 40 μM etomoxir in a non-CO_2 incubator at 37 °C. 1 mM palmitate conjugated to 0.17 mM BSA or BSA control was added to respective wells immediately before OCR measurement on XF-96 analyzer (Seahorse Bioscience).

ROS measurement. For mitochondrial and intracellular ROS measurements, macrophages were seeded at 1×10^5 cells per well in a 96-well plate and polarized toward M1 and M2 as described above. Macrophages were then washed with warm PBS and incubated at 37 °C with 5 μM MitoSox (Invitrogen), mitochondrial superoxide indicator, or 10 μM CM-H_2DCFDA (Invitrogen), cytosolic ROS indicator, in serum-free phenol red-free RPMI 1640 (Life Technologies) for 15 or 30 min respectively. Following washing, the fluorescence intensity of MitoSox and CM-H_2DCFDA were measured on a ClarioStar plate reader at excitation/emission spectra of 510/580 nm or 495/520 nm respectively. Extracellular ROS kinetics was assessed using a horseradish peroxidase (HRP)-luminol-dependent chemiluminescence method. 2×10^6 cells per well were plated in a 6-well plate and polarized toward M1 and M2 and treated before assay with 20 μM C75, 100 μM etomoxir or 500 μM mitoTEMPO as indicated in the figure legends. Macrophages were harvested, washed in PBS then re-suspended in PBS (with added $CaCl_2$ and $MgCl_2$) using 5×10^5 cells per assay sample; for human macrophages 2.5×10^5 cells were used. 1 μM Luminol and 62.5 U/ml HRP were added to the cell suspension for 3 min and cells were then transferred to a white 96-well luminometer plate (Berthold Technologies). 200 ng/ml PMA, 200 μg/ml serum-opsonized zymosan or PBS control was added directly to each well and light emission recorded by a Berthold Centro LB 960 luminometer (Berthold Technologies). Experiments with mouse and human neutrophils were similarly performed.

***In vitro* infection assay.** Macrophages were infected with *S.* Typhimurium SL1344 for 45 min at MOI 10 in media containing 10% FCS or serum free media (Opti-MEM 1). Cells were then washed and maintained for a further 45 min with media containing 50 μg/ml gentamicin before replacing for media without antibiotics. After 2 h, cells were washed with PBS and lysed with 0.1% Triton X-100 before plating serial dilutions in triplicate onto selective agar. For infection with the *Mycobacterium bovis* bacillus Calmette-Guérin (BCG) strain, macrophages were infected with BCG containing a luciferase reporter for 0, 4 or 24 h (ref. 30). Cells were then washed and lysed and relative light units (RLU), as direct correlates of colony-forming units (CFU), were measured as described[30].

***In vitro* macrophage cytokine-stimulation assay.** 1.5×10^5 macrophages per well were seeded in a 96-well plate. Cells were then washed and pre-treated with 20 μM C75, 100 μM etomoxir or vehicle only for 2 h and then stimulated with 200 μg/ml zymosan or 1 μg/ml of LPS. Supernatants were collected after 24 h and measured for IL-1β, IL-6, CXCL1 and TNF with ELISA according to the manufacturer's instructions (BD Bioscience).

***In vivo* endotoxin administration.** *E. coli* LPS (2 mg/kg or 10 mg/kg) was injected intraperitoneally into mice. All mice were male and between 5 weeks and 8 weeks of age. At indicated time points following intraperitoneal injection of LPS, serum was obtained by intracardiac puncture under terminal isoflurane anesthesia and mice were sacrificed. A graded scoring system, adapted from a published system[50], was employed to monitor the clinical severity of sepsis every 15 min following LPS injection, which consisted of scoring of respiration rate and breathing pattern (0–5), activity and movement (0–5) and appearance, including changes to coat and eyes (0–5), conducted by two scientists independently.

Immunoblot analysis. Cells were washed once in ice-cold PBS and lysed in RIPA buffer (50 mM Tris pH 7.4, 150 mM NaCl, 1% Igepal, 0.5% sodium deoxycholate, 0.1% SDS) with protease (Thermo Fisher Scientific, 78410) and phosphatase inhibitors (Thermo Fisher Scientific, 78426). Protein concentration was determined by BCA assay (Thermo Fisher Scientific, 23225) and equal amounts of proteins loaded onto SDS polyacrylamide gels. The proteins were transferred onto nitrocellulose membrane using a Trans-Blot Turbo transfer system (Bio-Rad). Membranes were incubated overnight with primary antibody, followed by corresponding secondary antibody, and the membranes were developed using 20X LumiGLO Reagent (Cell Signaling, 7003S).

Immunoprecipitation. Cells were washed three times with ice-cold PBS and then directly lysed with Tris-Triton buffer (10 mM Tris pH 7.4, 100 mM NaCl, 1 mM EDTA, 1 mM EGTA, 1% Triton-X100, 10% glycerol, 0.1% SDS, 0.5% deoxycholate) with added protease (Thermo Scientific, 78410) and phosphatase (Thermo Scientific, 78426) inhibitor cocktails. Lysed cells were centrifuged at 9,300*g* for 5 min at 4 °C to remove cell debris. Lysates were pre-cleared with either rabbit or mouse IgG bound to protein A sepharose beads (GE Healthcare, 17-5138-01) suspended in a 10% BSA-PBS solution rotated for 30 min at 4 °C. Pre-cleared lysates were added to protein A sepharose beads coated with a precipitation antibody (1:100) and were rotated at 4 °C for 1 h. Beads were washed with lysis buffer and the bound proteins were analyzed by immunoblot.

Precipitation of IL-1β from supernatants. Equal volumes of supernatants were precipitated using the TCA-DOC method. 1/100 of 2% sodium deoxycholate was added to one volume of the supernatant, vortexed and left for 30 min at 4 °C. Next, 1/10 of trichloroacetic acid was added, then samples were vortexed and left overnight at 4 °C. Samples were then spun down for 15 min at 4 °C at 15,000*g*. Pellets were washed once with one volume of ice cold acetone, air dried, resuspended in 2× loading buffer (4% SDS, 120 mM Tris HCl pH 6.8, 10% glycerol, 100 mM DTT and 100 μg of bromphenol blue), boiled for 5 min and separated by SDS-PAGE for further analysis.

Silver staining. Polyacrylamide gels were fixed for 1 h at 20 °C in 40% ethanol with 10% acetic acid. Gels were washed overnight with distilled water and then sensitized with 0.02% sodium thiosulphate for 1 min, washed and then stained for 20 min at 4 °C with 0.1% silver nitrate with 0.02% formaldehyde. Gels were developed with 3% sodium carbonate with 0.05% formaldehyde and staining was terminated with 5% acetic acid for 5 min.

Immunofluorescence staining. Cells were seeded on glass coverslips and differentiated overnight as required. Cells were fixed with 4% paraformaldehyde containing either 0.2% or 1% Triton X-100 for 15 min at 20 °C or 100% methanol at −20 °C for 15 min. Fixed cells were washed with PBS and non-specific binding was blocked with either 5% normal serum or 0.5% milk before incubation with primary antibodies for 1 h at 20 °C. Unbound antibody was removed by washing with PBS and secondary antibody was bound for 30 min at 20 °C. Coverslips were then mounted with either Prolong or Mowiol mountant containing DAPI. Fluorescence was visualized with a Zeiss LSM 510 or a DeltaVision Spectris Deconvolution Microscope.

Proximity-ligation assay. Cells were fixed and stained with primary antibody as described above for immunofluorescence. Proximity-ligation assay (PLA) was performed as per the manufacturer's instructions (Duolink *In situ*, Olink Bioscience). In brief, unbound antibody was removed by washing twice for 5 min with 1× wash buffer A and PLA probes were bound for 1 h at 37 °C. Unbound PLA probes were removed by washing twice for 5 min with 1× wash buffer A. Coverslips were incubated with Ligation-Ligase solution for 30 min at 37 °C. Ligation-Ligase solution was removed by washing twice for 2 min with 1× wash buffer A and coverslips were incubated with Amplification-Polymerase solution for 100 min at 37 °C. Amplification-Polymerase solution was removed first by washing twice for 10 min with 1× wash buffer B and second by washing 1 min with 0.01% wash buffer B. Coverslips were then mounted and fluorescence was visualized as described for immunofluorescence staining.

Oil Red O staining. Macrophages were seeded onto glass coverslips and allowed to differentiate overnight. Cells were washed twice with PBS and then incubated for 3 min in 100% propylene glycol (VWR) before staining with Oil Red O solution (0.5% Oil Red O [Amresco] in propylene glycol) for 10 min at 20 °C. Excess stain was removed by washing with 85% propylene glycol and washing with distilled water. Cells were counterstained with hematoxylin and mounted with Kaiser's glycerol gelatine (Merck Millipore).

Transmission electron microscopy. Cells were fixed in 4% glutaraldehyde in 0.1 M HEPES (pH 7.4) for 12 h at 4 °C, washed with 0.1M HEPES 5 times and then treated with 1% osmium ferricyanide at 20 °C for 2 h. Cells were rinsed in water five times and treated with 2% uranyl acetate in 0.05 M maleate buffer (pH 5.5) for 2 h at 20 °C, rinsed and dehydrated in an ascending series of ethanol solutions (70% to 100%) and then were treated with two changes of dry acetonitrile before infiltration with Quetol epoxy resin. Images were taken in an FEI Tecnai G2 operated at 120 Kv using an AMT XR60B digital camera running Deben software.

Quantitative real-time PCR. Total RNA was isolated from cultured cells and tissues using RNeasy Mini Kit (QIAGEN) according to the manufacturer's instructions. For RT-PCR, cDNA was synthesized using oligo(dT) primers and M-MLV reverse transcriptase followed by quantitative PCR analysis. The primers are shown in **Supplementary Table 5**.

Statistical analysis. Statistical significance was calculated as appropriate using an unpaired, two-tailed Student's *t*-test, Mann-Whitney *U*-test or analysis of variance and Bonferroni's test and Grubb's test for outlier exclusion, as described in the figure legends. Data is represented as mean and s.e.m. (s.e.m.). A P value of <0.05 was considered significant. Data were analyzed with Graphpad Prism software (version 6).

48. Cong, L. *et al.* Multiplex genome engineering using CRISPR/Cas systems. *Science* **339**, 819–823 (2013).
49. Behringer, R., Gertsenstein, M., Vintersten Nagy, K. & Nagy, A. *Manipulating the Mouse Embryo: A Laboratory Manual* 4th edn. 92–93, 139–142 and 211–215 (Cold Spring Harbor Laboratory Press, Cold Spring Harbor, New York, 2014).
50. Bougaki, M. *et al.* Nos3 protects against systemic inflammation and myocardial dysfunction in murine polymicrobial sepsis. *Shock* **34**, 281–290 (2010).

doi:10.1038/ni.3532